

UNCLASSIFIED

AD NUMBER
AD809384
NEW LIMITATION CHANGE
TO Approved for public release, distribution unlimited
FROM Distribution authorized to U.S. Gov't. agencies and their contractors; Specific authority; Nov 1966. Other requests shall be referred to Air Force Flight Dynamics Laboratory Research and Technology Division, AFSC, Wright-Patterson AFB, OH 45433.
AUTHORITY
AFFDL ltr, 24 Jan 1973

THIS PAGE IS UNCLASSIFIED

AFFDL-TR-66-105

809384

**INVESTIGATION OF CROSS WIND EFFECTS ON
STABLE PARACHUTE POINT-MASS SYSTEMS**

**H. G. HEINRICH
T. C. NIETZ**

UNIVERSITY OF MINNESOTA

TECHNICAL REPORT AFFDL-TR-66-105

NOVEMBER 1966

This document is subject to special export controls and each transmittal to foreign governments or foreign nationals may be made only with prior approval of the Vehicle Equipment Division (FDF), Air Force Flight Dynamics Laboratory, Wright-Patterson AFB, Ohio.

**AIR FORCE FLIGHT DYNAMICS LABORATORY
RESEARCH AND TECHNOLOGY DIVISION
AIR FORCE SYSTEMS COMMAND
WRIGHT-PATTERSON AIR FORCE BASE, OHIO**

**INVESTIGATION OF CROSS WIND EFFECTS ON
STABLE PARACHUTE POINT-MASS SYSTEMS**

*H. C. HEINRICH
T. C. NIETZ*

UNIVERSITY OF MINNESOTA

This document is subject to special export controls and each transmittal to foreign governments or foreign nationals may be made only with prior approval of the Vehicle Equipment Division (FDF), Air Force Flight Dynamics Laboratory, Wright-Patterson AFB, Ohio.

FOREWORD

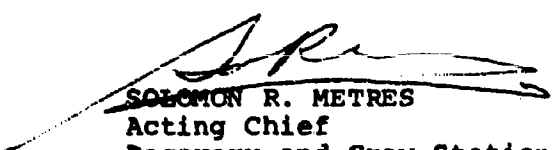
This report was prepared by the Department of Aeronautics and Engineering Mechanics of the University of Minnesota in compliance with U. S. Air Force Contract No. AF 33(615)-2554, "Theoretical Deployable Aerodynamic Decelerator Investigations," Task 606503, "Parachute Aerodynamics and Structures," Project 6065, "Performance and Design of Deployable Aerodynamic Decelerators."

The work accomplished under this contract was sponsored jointly by U. S. Army Natick Laboratory, Department of the Army; Bureau of Aeronautics and Bureau of Ordnance, Department of the Navy; and Air Force Systems Command, Department of the Air Force and was directed by a Tri-Service Steering Committee concerned with Aerodynamic Retardation. The work was administered under the direction of the Recovery and Crew Station Branch, Air Force Flight Dynamics Laboratory, Research and Technology Division. Mr. James H. DeWeese was the project engineer.

The authors wish to acknowledge the contributions by Messrs E. L. Haak and R. J. Niccum to this study and the assistance rendered by students of Aerospace Engineering of the University of Minnesota, particularly Messrs. James W. Hakanson and Thomas F. Goodrick.

The manuscript was released by the authors in April 1966 for publication as an RTD technical report.

This technical report was reviewed and is approved.



SOLOMON R. METRES
Acting Chief
Recovery and Crew Station Branch
AF Flight Dynamics Laboratory

ABSTRACT

The influence of horizontal wind shear layers upon descending, statically stable parachutes has been studied analytically and experimentally. The investigation was concerned with horizontal displacements, response velocity, response time, and angle of attack. Experiments were conducted with two circular flat ribbon, two ringslot, and one ribless guide surface parachute model. The results show that the analytical predictions are a satisfactory first approximation of the observed performance characteristics.

TABLE OF CONTENTS

	Page
I. Introduction	1
II. Theoretical Analysis	3
A. Derivation of Equations	3
B. Example Calculations	22
III. Experiments	22
A. Introduction	22
B. Experimental Procedure	30
C. Results	31
D. Conclusions	47
IV. Experimental Apparatus and Procedure	47
A. Introduction	47
B. Models	47
C. Cross Wind Tunnel	48
D. Catapult	56
E. Experimental Procedure	56
V. References	64

ILLUSTRATIONS

FIGURE		PAGE
1.	Trajectory of a Point-Mass Parachute in Wind Shear Layer	2
2.	Parachute Velocity and Angular Orientation	4
3.	Various Types of Wind Shear Layers	5
4.	Relative Wind Acting on Parachute	6
5.	Parachute Wind Response in Constant Wind Shear Layer	13
6.	Parachute Wind Response in Gradient Wind Shear Layer	14
7.	Altitude or Time Versus Parachute and Wind Velocity for Constant Shear Layer	17
8.	Altitude or Time Versus Parachute and Wind Velocity for Gradient Wind Layer	19
9.	Effect of Apparent Mass on a Parachute's Horizontal Velocity and Response Time	21
10.	Horizontal Velocity as a Function of Altitude of Point-Mass Parachute System at Various Terminal Velocity Conditions, Wind Gradient (γ) = 0.1 ft/sec/ft ($0 < h < 400$), Wind Velocity (V_w) = 40 ft/sec ($400 < h < 800$)	23
11.	Trajectory for Point-Mass Parachute System at Various Terminal Velocity Conditions, Wind Gradient (γ) = 0.1 ft/sec/ft ($0 < h < 400$), Wind Velocity (V_w) = 40 ft/sec ($400 < h < 800$)	24
12.	Angle of Relative Wind as a Function of Altitude for Point-Mass Parachute System at Various Terminal Velocity Conditions, Wind Gradient (γ) = 0.1 ft/sec/ft ($0 < h < 400$), Wind Velocity (V_w) = 40 ft/sec ($400 < h < 800$)	25
13.	Horizontal Velocity as a Function of Altitude for a Point-Mass Parachute System at Various Terminal Velocity Conditions, Wind Gradient (γ) = 0.1 ft/sec/ft	26

ILLUSTRATIONS (CONT.)

FIGURE	PAGE
14.	Horizontal Velocity as a Function of Altitude for a Point-Mass Parachute System at Various Terminal Velocity Conditions, Wind Velocity (V_w) = 10 ft/sec 27
15.	Horizontal Velocity as a Function of Altitude for a Point-Mass Parachute System at Various Terminal Velocity Conditions, Wind Velocity (V_w) = 20 ft/sec 28
16.	Horizontal Velocity as a Function of Altitude for a Point-Mass Parachute System at Various Terminal Velocity Conditions, Wind Velocity (V_w) = 40 ft/sec 29
17.	Trajectory of Various Parachutes, Terminal Velocity (V_{zp}) = 20 ft/sec Wind Velocity (V_w) = 37 ft/sec 32
18.	Trajectory of Various Parachutes, Terminal Velocity (V_{zp}) = 30 ft/sec Wind Velocity (V_w) = 37 ft/sec 33
19.	Trajectory of Various Parachutes, Terminal Velocity (V_{zp}) = 40 ft/sec Wind Velocity (V_w) = 37 ft/sec 34
20.	Horizontal Velocity as a Function of Altitude for Various Parachutes, Terminal Velocity (V_{zp}) = 20 ft/sec Wind Velocity (V_w) = 37 ft/sec 35
21.	Horizontal Velocity as a Function of Altitude for Various Parachutes, Terminal Velocity (V_{zp}) = 30 ft/sec Wind Velocity (V_w) = 37 ft/sec 36
22.	Horizontal Velocity as a Function of Altitude for Various Parachutes, Terminal Velocity (V_{zp}) = 40 ft/sec Wind Velocity (V_w) = 37 ft/sec 37
23.	Angle of Attack as a Function of Altitude for Various Parachutes, Terminal Velocity (V_{zp}) = 20 ft/sec Wind Velocity (V_w) = 37 ft/sec 38

ILLUSTRATIONS (CONT.)

FIGURE		PAGE
24.	Angle of Attack as a Function of Altitude for Various Parachutes, Terminal Velocity (v_{zp}) = 30 ft/sec Wind Velocity (v_w) = 37 ft/sec.	39
25.	Angle of Attack as a Function of Altitude for Various Parachutes, Terminal Velocity (v_{zp}) = 40 ft/sec Wind Velocity (v_w) = 37 ft/sec.	40
26.	Angle of Relative Wind as a Function of Altitude for Various Parachutes, Terminal Velocity (v_{zp}) = 20 ft/sec Wind Velocity (v_w) = 37 ft/sec.	41
27.	Angle of Relative Wind as a Function of Altitude for Various Parachutes, Terminal Velocity (v_{zp}) = 30 ft/sec Wind Velocity (v_w) = 37 ft/sec.	42
28.	Angle of Relative Wind as a Function of Altitude for Various Parachutes, Terminal Velocity (v_{zp}) = 40 ft/sec Wind Velocity (v_w) = 37 ft/sec.	43
29.	Angle of Attack as a Function of Time for the Ribless Guide Surface and 15% Ringslot Parachute at Various Terminal Velocity Conditions, Wind Velocity (v_w)=37 ft/sec. . .	44
30.	Orientation of Parachute and Relative Wind Vector in Experiments	45
31.	Circular Flat Ribbon and Ringslot Parachute Models	49
32.	Gore Patterns for Circular Flat Ribbon and Ringslot Parachute Models	50
33.	Ribless Guide Surface Parachute Model	51
34.	Gore Patterns for Ribless Guide Surface Parachute Model	52
35.	Cross Wind Tunnel	53
36.	Nozzle Section of Cross Wind Tunnel	54
37.	Method of Achieving Various Velocity Profiles in Cross Wind Tunnel	55

ILLUSTRATIONS (CONT.)

FIGURE		PAGE
38.	Pneumatic Catapult for Accelerating Parachutes to Terminal Velocity Conditions	57
39.	Parachute Model in Launch Configuration . .	58
40.	Experimental Set-Up for Determining Parachute Trajectories	59
41.	Catapult Systems and Cross Wind Tunnel . . .	60
42.	Timing Equipment for Determining Injection Velocities	62
43.	Photographic Sequence of Parachute Trajectory	63

SYMBOLS

C_D	drag coefficient
C_m	moment coefficient
\bar{D}	aerodynamic drag force
\bar{F}	total forces acting on parachute-load system
\bar{F}_A	apparent mass force
g	gravity
h	altitude
h_0	reference altitude (shear layer boundary)
\hat{i}	unit vector in horizontal direction
\hat{k}	unit vector in vertical direction
m	mass of suspended load
m'	apparent mass
S	area
t	time
t_r	response time
T	nondimensional time
\hat{v}	unit vector in direction of relative wind
\bar{V}_p	parachute velocity
V_{xp}	horizontal component of parachute velocity
V_{zp}	vertical component of parachute velocity
V_{xp0}	initial horizontal parachute velocity
\bar{V}_R	relative wind velocity
\bar{V}_W	wind velocity
V_{xw}	non-steady wind velocity
V_{xw0}	initial wind velocity

SYMBOLS (CONT.)

W	weight of parachute load
X_p	horizontal parachute displacement
α	angle of attack
γ	wind gradient
θ	parachute inclination angle
λ	geometric porosity
ρ	air density
ϕ	angle of relative wind

Subscripts

o	initial conditions of reference altitude
t	total of system

Additional symbols are defined in the text when they occur.

I. INTRODUCTION

The motions of a parachute-load system in a nearly vertical steady descent can be determined relatively easily by coupling of the known steady state aerodynamic characteristics (Ref 1) with the methods which lead to the prediction of the theory of dynamic stability behavior (Ref 2). When descending from a higher altitude, the steady descent is very likely to be interrupted by horizontal wind fields known as wind shear layers. Upon entering such a shear layer, the parachute system is subjected to an initial angle of attack. Subsequent motions will be a combination of angular and lateral displacements as shown in Fig 1. The magnitude of these oscillations and displacements will depend, in part, on canopy type, equilibrium velocity, damping, strength of the wind field, its gradient with respect to altitude, and apparent mass effects.

In view of these facts, a study was conducted at the University of Minnesota to determine analytically and experimentally the trajectory characteristics of a stable parachute-load configuration under the influence of shear layers with constant and varying strengths.

Experimental investigations were limited to five parachutes, two circular flat ribbon and two ringslot canopy types, each of 15 and 25 percent total porosity, and one ribless guide surface canopy with a cloth permeability of 120. Parachutes were vertically injected into a horizontal flow wind tunnel. In this manner, the wind initially acted normal to the longitudinal axis of the parachute canopy. The cross wind velocities included a steady wind field of 37 ft/sec and a non-steady layer varying nearly linearly between 5 and 45 ft/sec. The parachutes were injected into the constant flow field at 20, 30, and 40 ft/sec, and they were injected into the varying flow layer at 15 ft/sec.

Under the assumption of a steady rate of descent, the constant and the varying horizontal flow fields may also be considered as steady and non-steady gusts, when recorded by an observer positioned on the descending parachute-load system.

The analytical study of the flight path of the parachute-load combination was pursued in view of an investigation concerning the wind response error of rising spherical balloons (Ref 3). A solution has been obtained in the following chapters for angular and horizontal displacement, wind response, and response time for the parachute-load system. In a number of cases a comparison between calculated and observed behavior has been accomplished. The agreement is, in general, satisfactory.

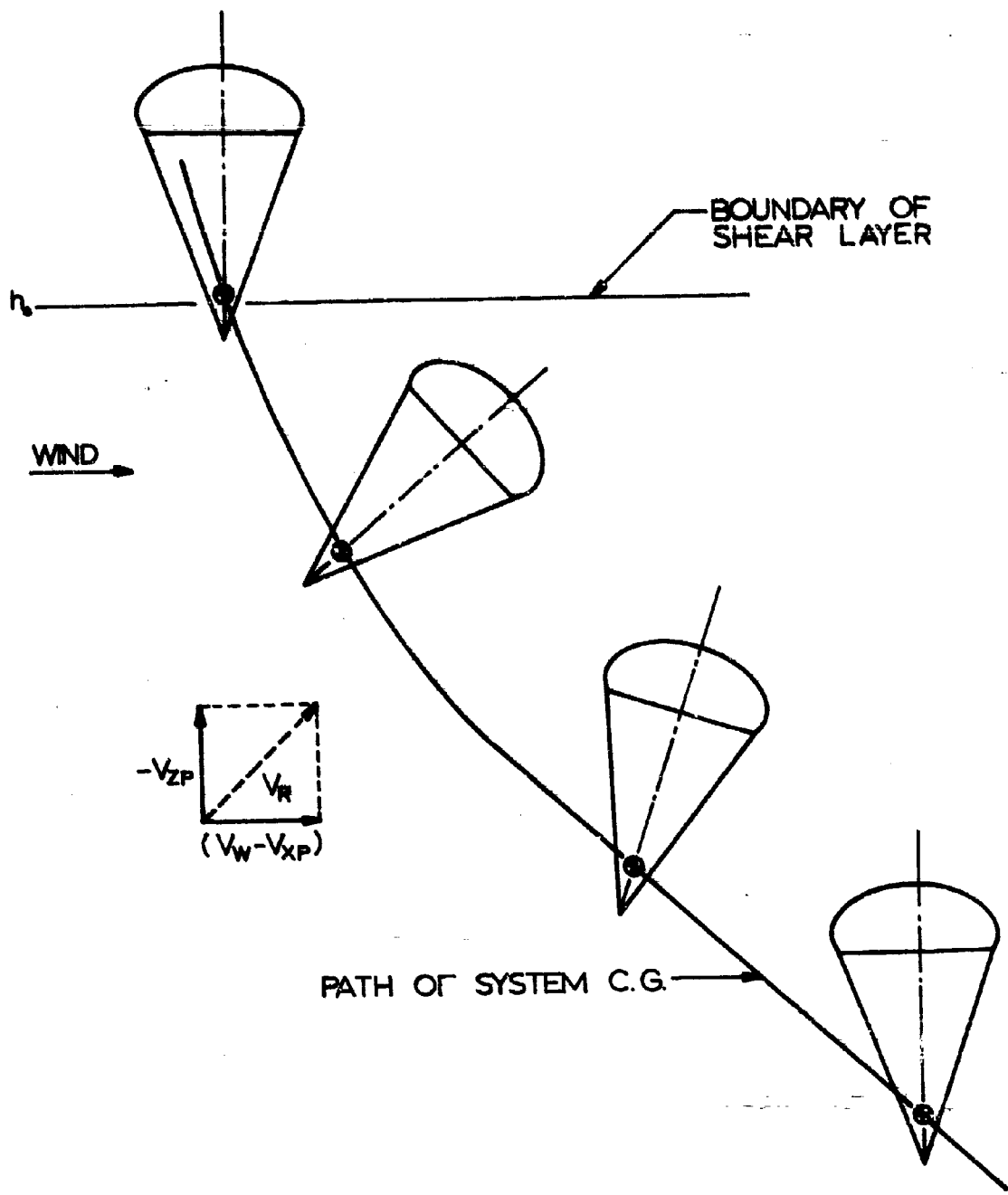


Fig 1. Trajectory of a Point-Mass Parachute in Wind Shear Layer

II. THEORETICAL ANALYSIS

A. Derivation of Equations

When a descending parachute enters a horizontal wind field, the parachute-load system will accelerate as it passes through the shear layer. If the parachute motion is restricted to the x-z plane, as in Fig 2, the velocity may be written in component form as:

$$\vec{V}_p = V_{xp}\hat{i} + V_{zp}\hat{k}. \quad (1)$$

The horizontal wind field can be represented by a constant or a varying shear layer, as shown in Fig 3. In general, the wind profile is written with steady and non-steady terms as follows:

$$\vec{V}_w = (V_{xw_0} + V_{xw}) \hat{i}. \quad (2)$$

Introducing the wind gradient $\gamma = dV_{xw}/dh$, one can write the non-steady wind term as $V_{xw} = \gamma (h-h_0)$. Whereupon, the complete wind profile becomes:

$$\vec{V}_w = [V_{xw_0} + \gamma(h - h_0)] \hat{i}. \quad (3)$$

It is also necessary to consider the relative wind which is the difference between wind and parachute velocities, as shown in Fig 4, or:

$$\vec{V}_R = (\vec{V}_w - \vec{V}_p), \quad (4)$$

and expanding Eqn 4:

$$\vec{V}_R = (V_w - V_{xp}) \hat{i} - V_{zp}\hat{k}, \quad (5)$$

from which the magnitude of the relative wind follows as:

$$|V_R| = \left[(V_w - V_{xp})^2 + V_{zp}^2 \right]^{\frac{1}{2}}, \quad (6)$$

and a unit vector in the direction of the relative wind becomes:

$$\hat{v} = \vec{V}_R / |V_R|. \quad (7)$$

The motion of a descending parachute is governed by Newton's Second Law, written symbolically as:

$$\sum \mathbf{F} = m_t \frac{d\vec{V}_p}{dt}, \quad (8)$$

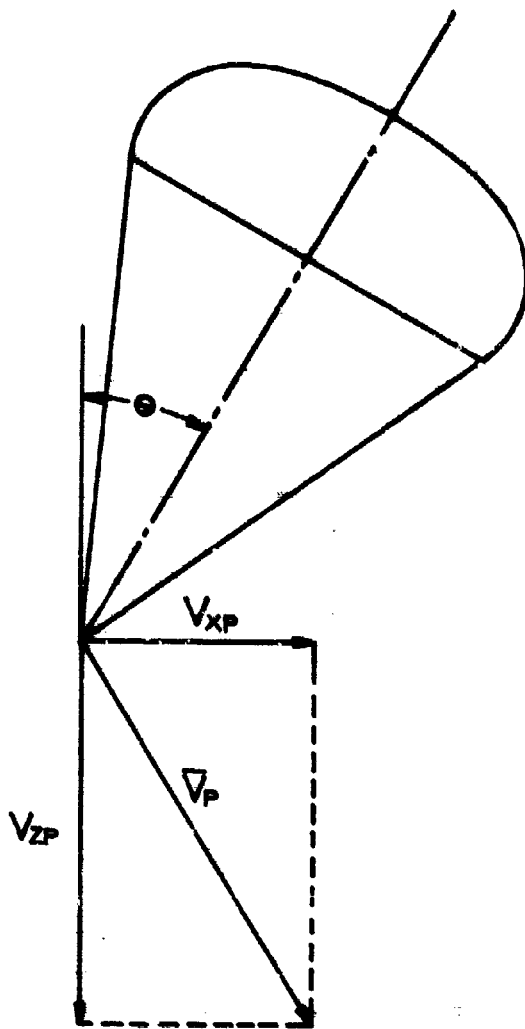


Fig 2. Parachute Velocity and Angular Orientation

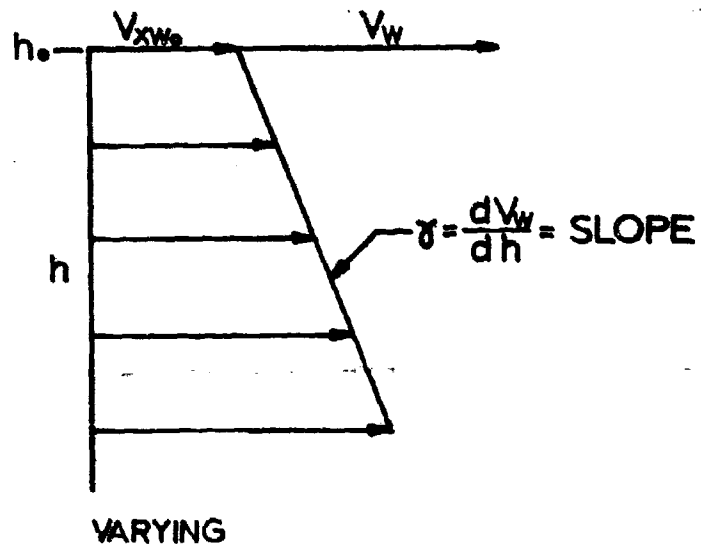
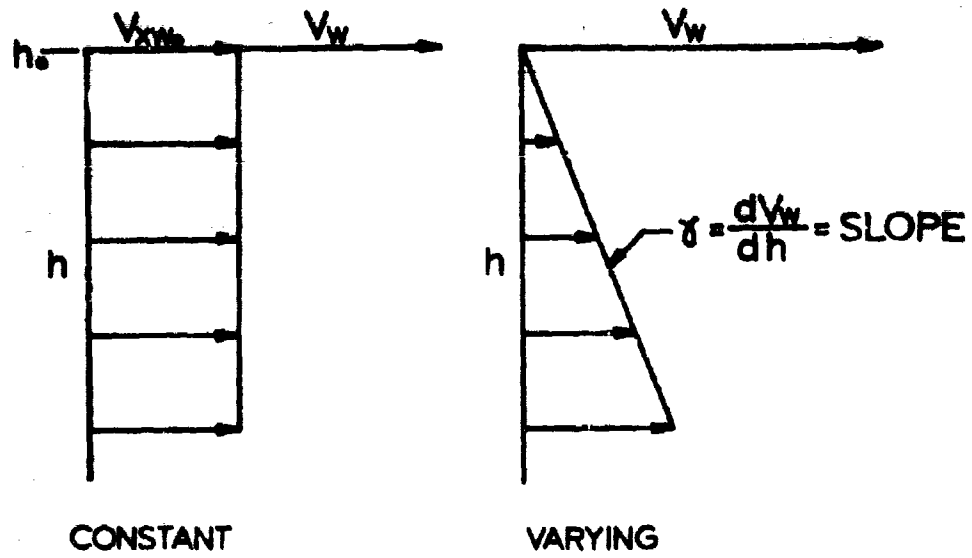


Fig 3. Various Types of Wind Shear Layers

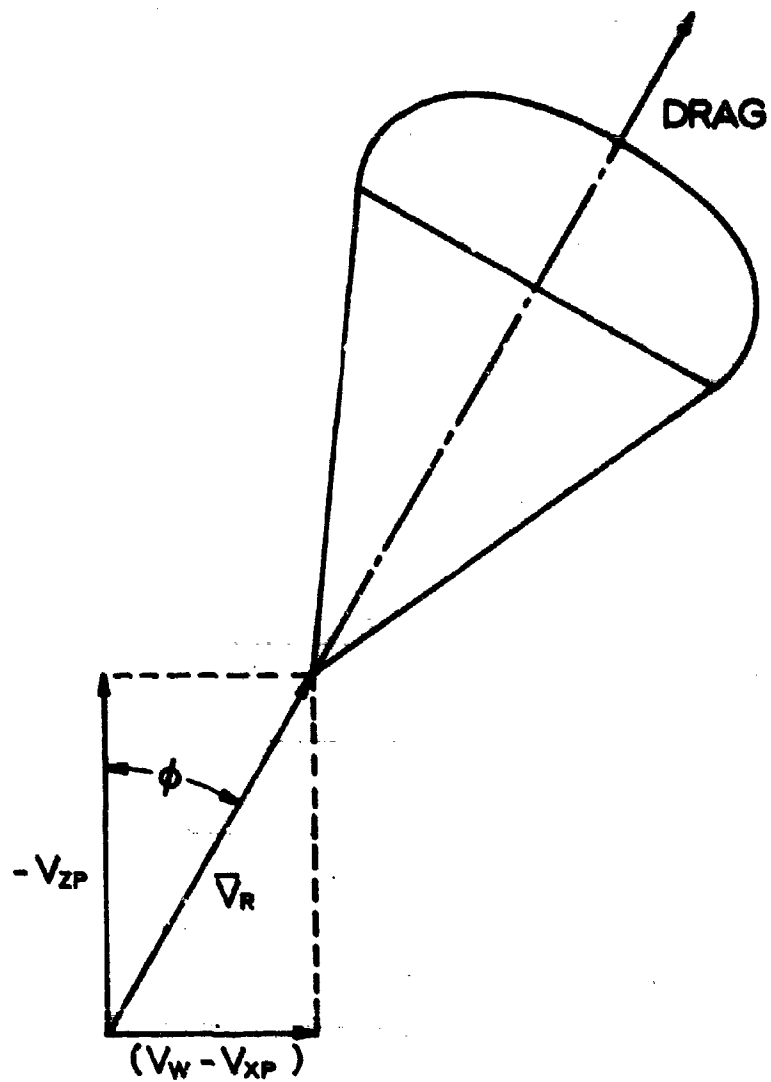


Fig 4. Relative Wind Acting on Parachute

where:

$\sum F$ = sum of all external forces

m_t = mass of parachute and load plus included mass

The external forces acting on the parachute are the aerodynamic drag, gravity, and the apparent mass effect. Mathematically, these may be expressed respectively as:

$$\sum F = D + W + F_A \quad (9)$$

To determine the aerodynamic drag, it is assumed that the strength of the wind shear layer increases gradually with altitude. Hence, dynamic effects can be neglected and the parachute will align itself with the relative wind velocity vector, as shown in Fig 4. The drag force is then written conventionally as:

$$D = C_D \frac{\rho}{2} S |V_R|^2 \hat{v} \quad (10)$$

or introducing Eqn 6 and 7 into Eqn 10, it follows:

$$D = C_D \frac{\rho}{2} S |V_R| [(v_w - v_{xp}) \hat{i} - v_{zp} \hat{k}] \quad (11)$$

The weight force acting on the system is:

$$W = mg \hat{k} \quad (12)$$

The apparent mass force arises from the transfer of kinetic energy from the parachute to the surrounding air (Refs 4 and 5). This effect is only noticeable while the parachute is accelerating or decelerating with respect to the air and is written:

$$F_A = m' \frac{d\vec{v}_R}{dt} \quad (13)$$

where m' is the apparent mass as determined from potential theory and experiments (Ref 6). By introducing Eqn 5, Eqn 13 becomes:

$$\vec{F}_A = m' (\dot{v}_w - \dot{v}_{xp}) \hat{i} - m' \dot{v}_{zp} \hat{k} \quad (14)$$

The equation of motion is now written using Eqns 11, 12, and 14,

$$\begin{aligned} \sum F &= m_t (\dot{v}_{xp} \hat{i} + \dot{v}_{zp} \hat{k}) \\ &= C_D \frac{\rho}{2} S |V_R| [(v_w - v_{xp}) \hat{i} - v_{zp} \hat{k}] \\ &\quad + mg \hat{k} + m' [(\dot{v}_w - \dot{v}_{xp}) \hat{i} - \dot{v}_{zp} \hat{k}] \end{aligned} \quad (15)$$

or in terms of the horizontal and vertical component directions, respectively:

$$m_t \dot{v}_{xp} = C_D \frac{\rho}{2} S |v_R| (v_w - v_{xp}) + m' (\dot{v}_w - \dot{v}_{xp}); \quad (16)$$

$$m_t \dot{v}_{zp} = - C_D \frac{\rho}{2} S |v_R| v_{zp} + mg - m' \dot{v}_{zp}. \quad (17)$$

It is further assumed that the parachute descends at a constant rate; hence, $\dot{v}_{zp} = 0$ and Eqn 17 may be solved for the relative wind.

$$|v_R| = \frac{mg}{C_D \frac{\rho}{2} S v_{zp}}. \quad (18)$$

Substituting this value of $|v_R|$ into Eqn 16 yields:

$$m_t \dot{v}_{xp} = \frac{mg}{v_{zp}} (v_w - v_{xp}) + m' (\dot{v}_w - \dot{v}_{xp});$$

or

$$(m_t + m') \dot{v}_{xp} - \frac{mg}{v_{zp}} v_w + \frac{mg}{v_{zp}} v_{xp} - m' \dot{v}_w = 0. \quad (19)$$

Equation 19 is a differential equation of v_{xp} with respect to time, which may be arranged in a more useful form with the following expressions:

$$\dot{v}_{xp} = \frac{dv_{xp}}{dt} = \frac{dv_{xp}}{dh} \frac{dh}{dt} = \frac{dv_{xp}}{dh} v_{zp};$$

$$\dot{v}_w = \frac{dv_w}{dt} = \frac{dv_w}{dh} \frac{dh}{dt} = \gamma v_{zp};$$

$$v_w = v_{xw_0} + \gamma(h - h_0).$$

Substituting the above relations into Eqn 19 yields:

$$\frac{dv_{xp}}{dh} - \frac{mg\gamma}{(m_t + m')v_{zp}^2} (h - h_0) + \frac{mg}{(m_t + m')v_{zp}^2} v_{xp} \quad (20)$$

$$- \left(\frac{mgv_{xw_0}}{(m_t + m')v_{zp}^2} + \frac{\gamma m'}{m_t + m'} \right) = 0$$

Since Eqn 20 is a differential equation of V_{xp} with respect to h only, a closed form solution can be found by standard methods (Ref 7). The solution is simplified with the following abbreviations.

$$P = \frac{mg}{(m+m')V_{zp}^2}$$

$$Z = \frac{mg\delta}{(m+m')V_{zp}^2}$$

$$Q = \frac{mgV_{xw_0}}{(m+m')V_{zp}^2} + \frac{\delta m'}{m+m'}$$

$$V = V_{xp}$$

$$Y = h - h_0$$

$$dY = dh.$$

Equation 20 can now be written as:

$$dV + [PV - Q - ZY] dY = 0 \quad (21)$$

Equation 21 is an exact differential equation which is solved as follows:

Multiply Eqn 21 by e^{PY} ;

$$e^{PY} dV + e^{PY} (PV - Q - ZY) dY = 0. \quad (22)$$

Letting:

$$M = e^{PY} (PV - Q - ZY) \quad (23)$$

$$N = e^{PY}, \quad (24)$$

Eqn 22 reduces to:

$$NdV + MdY = 0. \quad (25)$$

Writing a total differential equation as

$$dG = \frac{\partial G}{\partial V} dV + \frac{\partial G}{\partial Y} dY = 0, \quad (26)$$

where G is any arbitrary function, and comparing terms in Eqn 26 with those in Eqn 25, it is evident that:

$$\frac{\partial G}{\partial V} = e^{PY}, \quad (27)$$

$$\frac{\partial G}{\partial Y} = e^{PY} (PV - Q - ZY). \quad (28)$$

Integrating Eqn 27 yields:

$$G = V e^{PY} + f(Y), \quad (29)$$

and differentiating Eqn 29 with respect to Y :

$$\frac{\partial G}{\partial Y} = PV e^{PY} + f'(Y). \quad (30)$$

Comparing Eqns 30 and 28, one finds:

$$PV e^{PY} + f'(Y) = e^{PY} PV - e^{PY} (Q + ZY), \quad (31)$$

which reduces to:

$$f'(Y) = - (Q + ZY) e^{PY}. \quad (32)$$

Integrating Eqn 32 yields:

$$f(Y) = \left(-\frac{ZY}{P} + \frac{Z}{P^2}\right) e^{PY} - \frac{Q}{P} e^{PY} + C_1, \quad (33)$$

where C_1 is an arbitrary constant of integration.

Now it is possible to complete Eqn 29, since $f(Y)$ is known. Hence,

$$G = V e^{PY} + e^{PY} \left(-\frac{Z}{P} Y + \frac{Z}{P^2} - \frac{Q}{P}\right) + C_1. \quad (34)$$

But Q and C_1 are both arbitrary and can be combined into a single constant, C_2 . Thus, Eqn 34 becomes:

$$0 = v e^{PY} + e^{PY} \left(-\frac{Z}{P^2} + \frac{Z}{P^2} - \frac{Q}{P} \right) + C_2, \quad (35)$$

and after rearranging terms, Eqn 35 becomes:

$$v = \frac{Q - Z/P}{P} + \frac{Z}{P} Y - C_2 e^{-PY}. \quad (36)$$

The solution is completed by introducing the initial parachute velocity at the boundary of the wind shear layer as:

$$v_{xp} = v_{xp_0} \quad \text{at} \quad h = h_0,$$

that is,

$$v = v_{xp_0} \quad \text{at} \quad Y = 0.$$

Therefore,

$$C_2 = \frac{Q - Z/P}{P} - v_{xp_0},$$

and

$$v = \frac{Q - Z/P}{P} (1 - e^{-PY}) + \frac{Z}{P} Y + v_{xp_0} e^{-PY}. \quad (37)$$

After substituting the respective values for Z , P , Q , Y , and v , Eqn 37 yields the horizontal parachute velocity as a function of altitude.

$$v_{xp} = v_{xw_0} + \gamma (h - h_0) + (v_{xp_0} - v_{xw_0}) \cdot \left[e^{\frac{-m}{m_t + m'} \frac{g}{v_{zp}^2} (h - h_0)} - \gamma \frac{m_t}{m} \frac{v_{zp}^2}{g} \left[1 - e^{\frac{-m}{m_t + m'} \frac{g}{v_{zp}^2} (h - h_0)} \right] \right]. \quad (38)$$

Equation 38 can be rearranged as follows to yield the wind response, sometimes called the wind response error,

$$V_{xw_0} + \gamma (h - h_0) - V_{xp} = (V_{xw_0} - V_{xp_0}) \cdot$$

$$\left[e^{\frac{-m}{m_t + m'} \frac{g}{v_{zp}^2} (h - h_0)} \right] + \gamma \frac{m_t}{m} \frac{v_{zp}^2}{g} \cdot$$

$$\left[1 - e^{\frac{-m}{m_t + m'} \frac{g}{v_{zp}^2} (h - h_0)} \right],$$

or by Eqn 3,

$$V_w - V_{xp} = (V_{xw_0} - V_{xp_0}) \left[e^{\frac{-m}{m_t + m'} \frac{g}{v_{zp}^2} (h - h_0)} \right]$$

$$+ \gamma \frac{m_t}{m} \frac{v_{zp}^2}{g} \left[1 - e^{\frac{-m}{m_t + m'} \frac{g}{v_{zp}^2} (h - h_0)} \right] \quad (39)$$

Physically the wind response is the velocity difference between the parachute and surrounding air. As the parachute enters a wind shear layer, the effect of the velocity difference is to accelerate the parachute. For a steady wind, the parachute accelerates until it moves with the wind, as shown in Fig 5. When the wind field is a varying shear layer, as in Fig 6, the parachute will accelerate to a maximum response, which for large values of $h - h_0$ becomes:

$$(V_w - V_{xp})_{\max} = \gamma \frac{m_t}{m} \frac{v_{zp}^2}{g}. \quad (40)$$

It is evident from Eqn 39 that the wind response depends strongly on the rate of descent, wind gradient and velocity differential between parachute and wind as the parachute enters the shear layer. The apparent mass influences the response error. However, this effect may be small for highly porous canopies, (Ref 6). In the calculations of Section III, the apparent and included masses were neglected because of insignificance.

If the analysis were applied to parachutes with specifically high apparent mass or meteorological balloons, the apparent mass should not be neglected, because the apparent mass effect is a driving force in addition to aerodynamic drag, thus effectively reducing the magnitude of the wind response.

Knowing the horizontal wind, the rate of descent, and the wind response, one can also compute the parachute inclination angle, θ , which, theoretically, is equal to the angle of relative wind as defined in Fig 4. Mathematically, the inclination angle is expressed by:

$$\theta = \tan^{-1} \left(\frac{V_w - V_{xp}}{v_{zp}} \right). \quad (41)$$

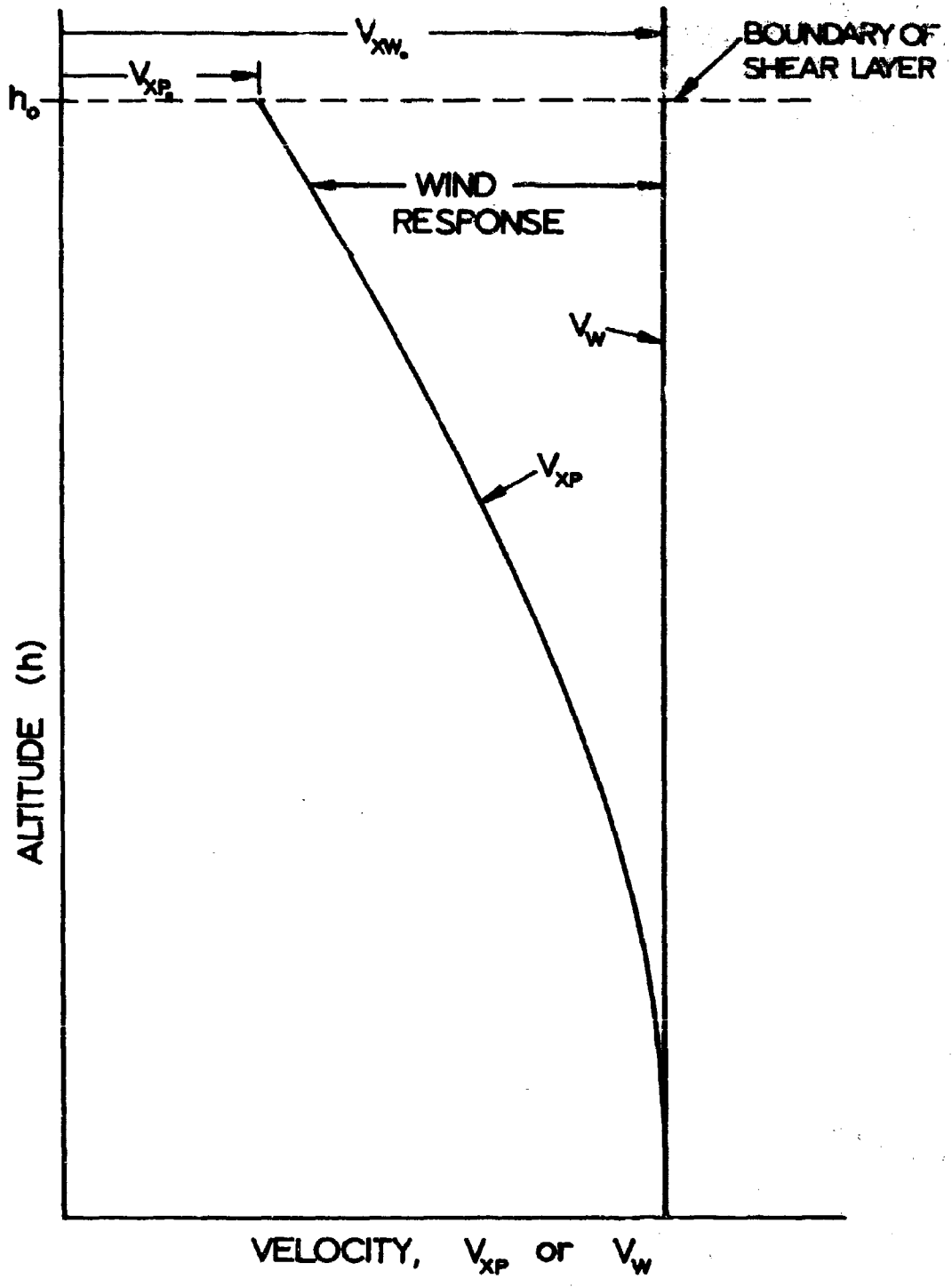


Fig 5. Parachute Wind Response in Constant Wind Shear Layer

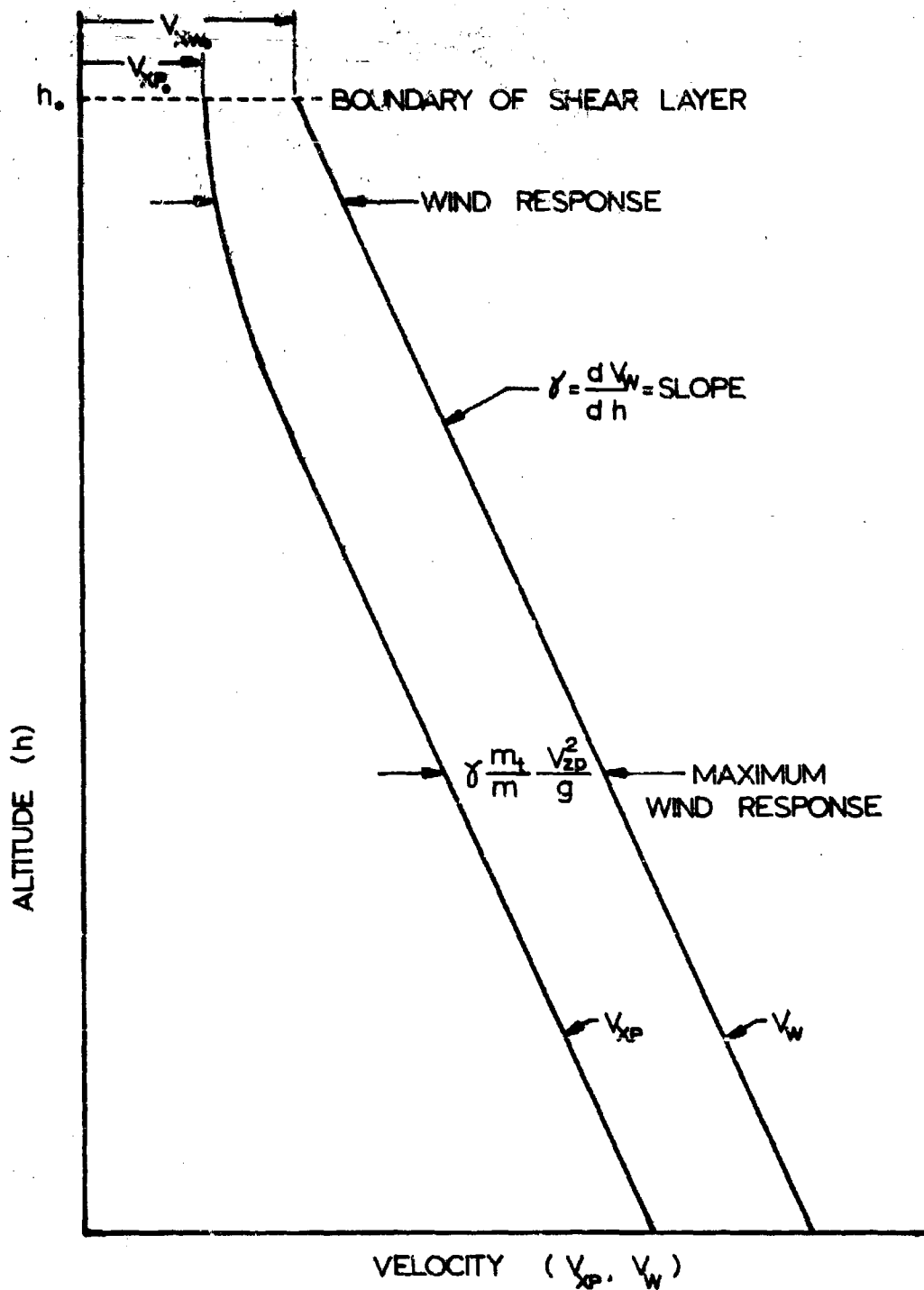


Fig 6. Parachute Wind Response in Gradient Wind Shear Layer

This relation follows if the parachute aligns itself instantaneously with the direction of the relative wind.

The horizontal parachute velocity, as expressed in Eqn 38, can be integrated again yielding the horizontal displacement or finally, the trajectory. This is accomplished after introducing the following terms:

$$v_{xp} = \frac{dx_p}{dt} = \frac{dx_p}{dh} \frac{dh}{dt} = \frac{dx_p}{dh} v_{zp}$$

$$Y = h - h_0$$

$$dY = dh$$

$$P = \frac{mg}{(m_t + m')v_{zp}^2}$$

Equation 38 is now written as:

$$dx_p = \left[\frac{\gamma}{v_{zp}} Y + \frac{v_{xp0}}{v_{zp}} e^{-PY} + \left(\frac{v_{xw0}}{v_{zp}} - \gamma \frac{m_t}{m} \frac{v_{zp}}{g} \right) \left(1 - e^{-PY} \right) \right] dY \quad (42)$$

where x_p is the parachute horizontal position. Integrating Eqn 42 leaves:

$$x_p = \frac{\gamma}{2v_{zp}} Y^2 - \frac{v_{xp0}}{Pv_{zp}} e^{-PY} + \left(\frac{v_{xw0}}{v_{zp}} - \gamma \frac{m_t}{m} \frac{v_{zp}}{g} \right) \left(Y + \frac{1}{P} e^{-PY} \right) + \frac{C_3}{v_{zp}} \quad (43)$$

The constant of integration, C_3 , is determined from the initial conditions:

$$x_p = 0 \text{ at } h = h_0, Y = 0.$$

Therefore:

$$C_3 = \frac{1}{P} (v_{xp0} - v_{xw0} + \gamma \frac{m_t}{m} \frac{v_{zp}^2}{g})$$

The trajectory equation is now written completely as:

$$\begin{aligned}
 x_p = & \frac{\gamma}{2v_{zp}} (h - h_0)^2 + \left(\frac{v_{xw_0}}{v_{zp}} - \gamma \frac{m_t}{m} \frac{v_{zp}}{g} \right) (h - h_0) \\
 & + \left[(v_{xp_0} - v_{xw_0} + \gamma \frac{m_t}{m} \frac{v_{zp}^2}{g}) \left(\frac{m_t + m'}{m} \right) \left(\frac{v_{zp}}{g} \right) \right] \cdot \quad (44) \\
 & \left[1 - e^{-\frac{m}{m_t + m'} \frac{g}{v_{zp}^2} (h - h_0)} \right].
 \end{aligned}$$

A superficial review of the wind response and trajectory equations might indicate that they are independent of canopy size, drag coefficient, weight, and air density. However, these terms are all incorporated within the terminal descent velocity v_{zp} , expressed conventionally as equilibrium speed

$$v_e = v_{zp} = \sqrt{\frac{2W}{C_D \rho S}}.$$

The wind response can also be expressed as a function of time by assuming that the rate of descent remains constant throughout the wind shear layer. Thus, the time required for the parachute to descend from h_0 to h becomes:

$$t = \frac{h - h_0}{v_{zp}} \quad (45)$$

Introducing Eqn 45 into Eqn 39 and after rearranging terms, the wind response takes the form:

$$v_w - v_{xp} = \left[(v_{xw_0} - v_{xp_0} - \gamma \frac{m_t}{m} \frac{v_{zp}^2}{g}) e^{-\frac{m}{m_t + m'} \frac{g}{v_{zp}^2} t} + \gamma \frac{m_t}{m} \frac{v_{zp}^2}{g} \right], \quad (46)$$

whereupon solving for t yields:

$$t = - \frac{m_t + m'}{m} \frac{v_{zp}}{g} \ln \left[\frac{v_w - v_{xp} - \gamma \frac{m_t}{m} \frac{v_{zp}^2}{g}}{v_{xw_0} - v_{xp_0} - \gamma \frac{m_t}{m} \frac{v_{zp}^2}{g}} \right]. \quad (47)$$

It is convenient to introduce a nondimensional time $T = t/t_r$, where the response time, t_r , is the time required for the parachute-load system to approach, to a certain degree, the steady state conditions after entering the shear layer. In this view, the response time for a constant shear layer, Fig 7, has been determined for the condition that the wind response diminishes to 5 percent

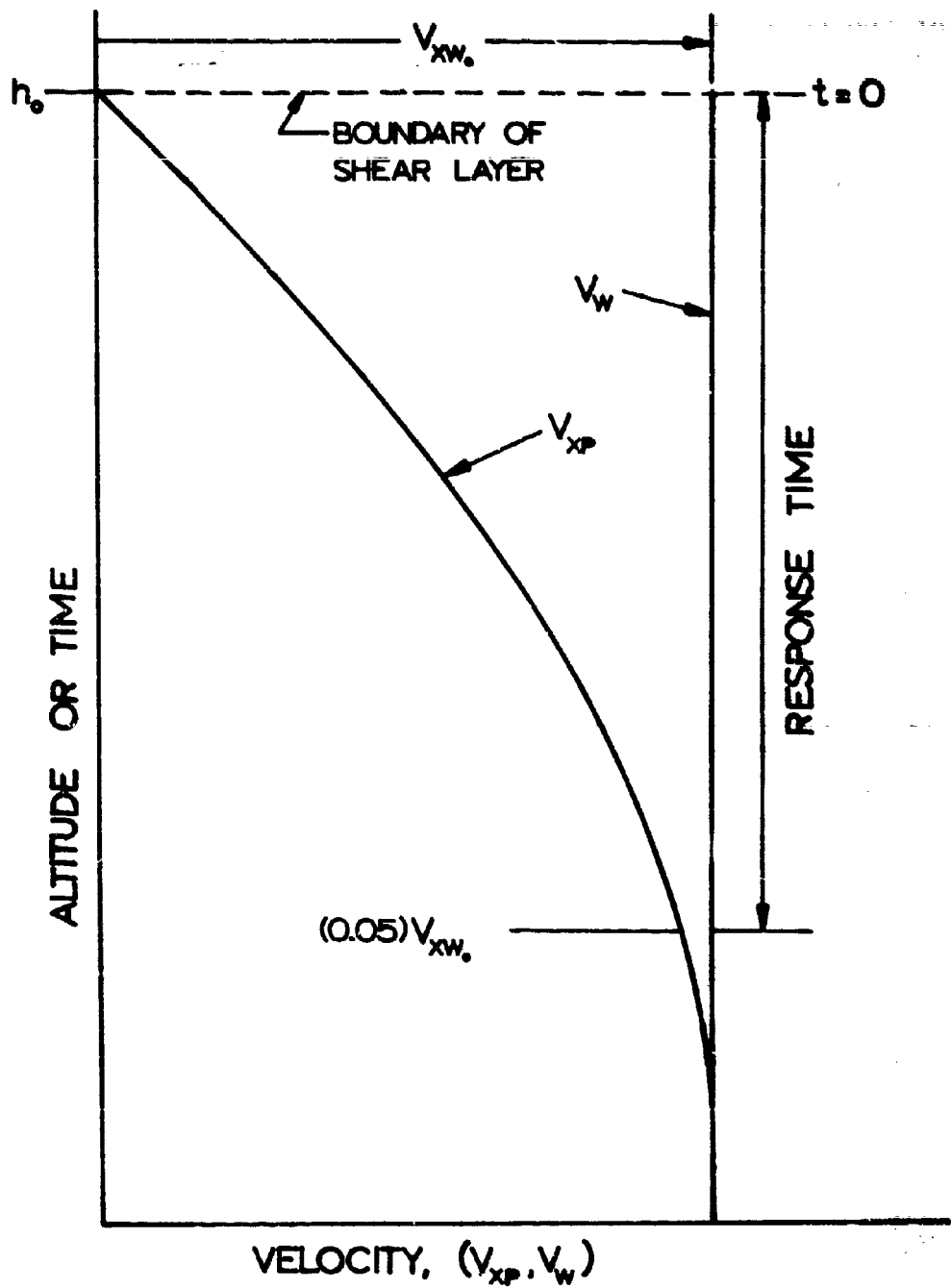


Fig 7. Altitude or Time Versus Parachute and Wind Velocity for Constant Shear Layer

of the horizontal wind velocity; or numerically,

$$\frac{V_{xw_0} - V_{xp}}{V_{xw_0}} = 0.05 .$$

A constant wind shear layer implies that the slope $\gamma = 0$, and assuming $V_{xp_0} = 0$, Eqn 47 reduces to:

$$t = - \frac{m_t + m' V_{zp}}{m} \frac{V_{zp}}{g} \ln \left(\frac{V_{xw_0} - V_{xp}}{V_{xw_0}} \right). \quad (48)$$

Subsequently, the response time is determined by introducing the 5 percent wind response requirement; hence,

$$t_r = - \frac{m_t + m' V_{zp}}{m} \frac{V_{zp}}{g} \ln (0.05), \quad (49a)$$

or

$$t_r = 3 \frac{m_t + m' V_{zp}}{m} \frac{V_{zp}}{g} . \quad (49b)$$

Thus, Eqn 49b is the response time for a parachute-load system in a constant wind shear layer, provided that the rate of descent remains constant throughout the entire layer. Continuing the analysis, the nondimensional time is now found by dividing Eqn 49b into Eqn 48, yielding:

$$T = \frac{t}{t_r} = - \frac{1}{3} \ln \left(\frac{V_{xw_0} - V_{xp}}{V_{xw_0}} \right). \quad (50)$$

It is interesting to note that the nondimensional time is a function of the wind and parachute velocities only. However, one must realize that the expression for horizontal parachute velocity, Eqn 38, contains all of the parameters of any real problem.

For a gradient shear layer, the response time has been defined as the time for the wind response to reach 95 percent of the maximum wind response value, as shown in Fig 8. The analysis proceeds by dividing the argument of Eqn 47 by the maximum wind response, $(V_w - V_{xp})_{\max}$, yielding,

$$t = - \frac{m_t + m' V_{zp}}{m} \frac{V_{zp}}{g} \ln \left[\frac{\frac{V_w - V_{xp}}{(V_w - V_{xp})_{\max}} - \frac{\gamma m_t V_{zp}^2 / mg}{(V_w - V_{xp})_{\max}}}{\frac{V_{xw_0} - V_{xp_0}}{(V_w - V_{xp})_{\max}} - \frac{\gamma m_t V_{zp}^2 / mg}{(V_w - V_{xp})_{\max}}} \right]. \quad (51)$$

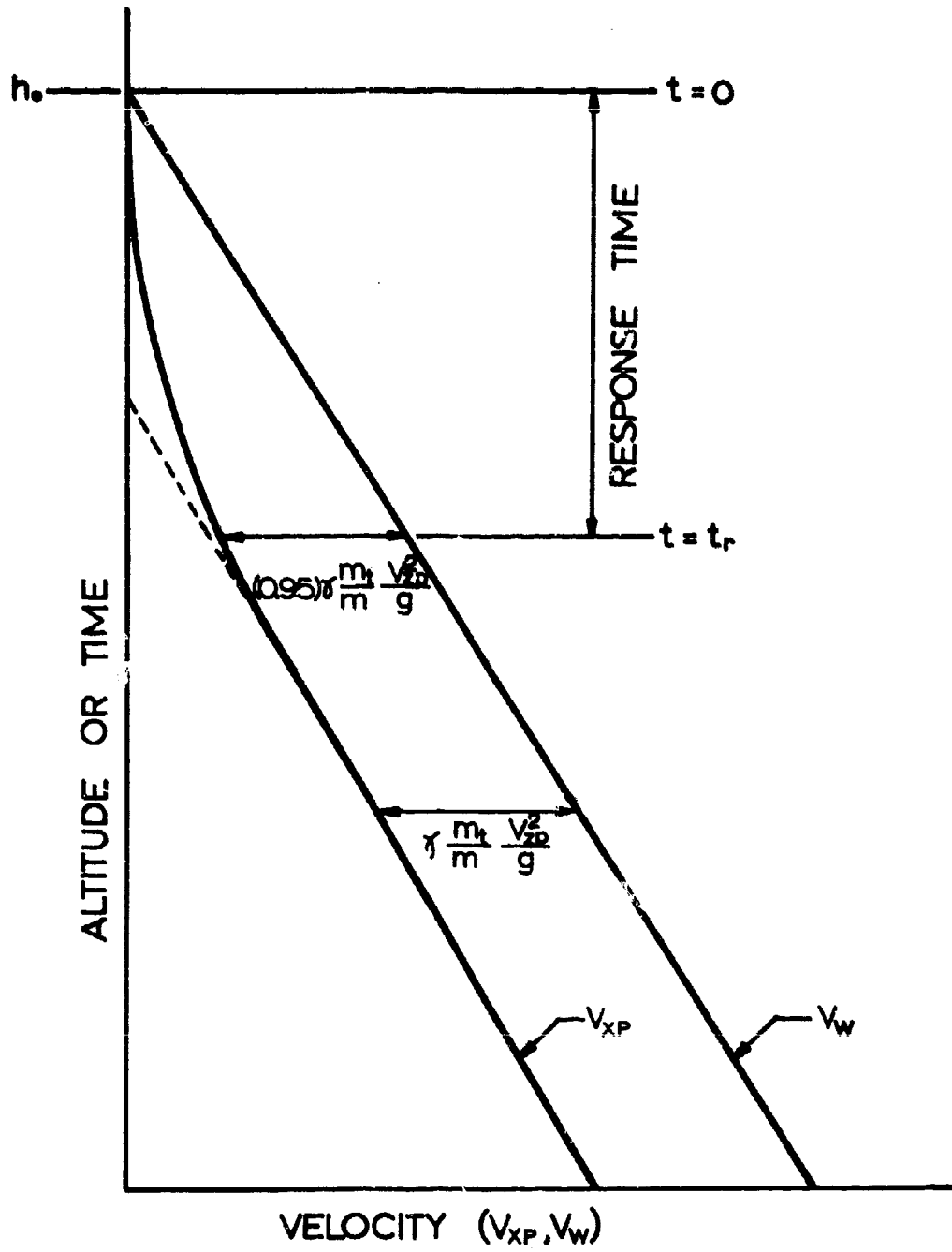


Fig 8. Altitude or Time Versus Parachute and Wind Velocity for Gradient Wind Layer

Recalling Eqn 40 and again assuming $V_{xp_0} = 0$ and $V_{xw_0} = 0$, Eqn 51 simplifies to:

$$t = - \frac{m_t + m'}{m} \frac{V_{zp}}{g} \ln \left[\frac{\frac{V_w - V_{xp}}{(V_w - V_{xp})_{\max}} - 1}{-1}} \right] \quad (52)$$

And introducing the 95 percent wind response requirement yields the response time in a gradient shear layer to

$$t_r = - \frac{m_t + m'}{m} \frac{V_{zp}}{g} \ln \left(- \frac{0.05}{-1} \right), \quad (53a)$$

or

$$t_r = 3 \frac{m_t + m'}{m} \frac{V_{zp}}{g}. \quad (53b)$$

The nondimensional time for gradient shear layer is obtained by dividing Eqn 53b into Eqn 52, leaving:

$$T = \frac{t}{t_r} = - \frac{1}{3} \ln \left[1 - \frac{V_w - V_{xp}}{(V_w - V_{xp})_{\max}} \right]. \quad (54)$$

In view of Eqn 49b and 53b, it is evident that the response times in steady and non-steady shear layers are identical to each other and independent of the strength of the shear layer. It is also interesting to note that the response time increases when apparent mass terms are introduced as shown in Fig 9. Disregarding the instant of the first impact of the parachute in the shear layer, the effect of apparent mass is a driving force for non-steady winds and a retarding force for steady winds; consequently, the response time increases in each case. For $h - h_0$ sufficiently large, the relative accelerations between parachute and wind vanish. Hence, the apparent mass force also vanishes and the final wind response becomes independent of apparent mass.

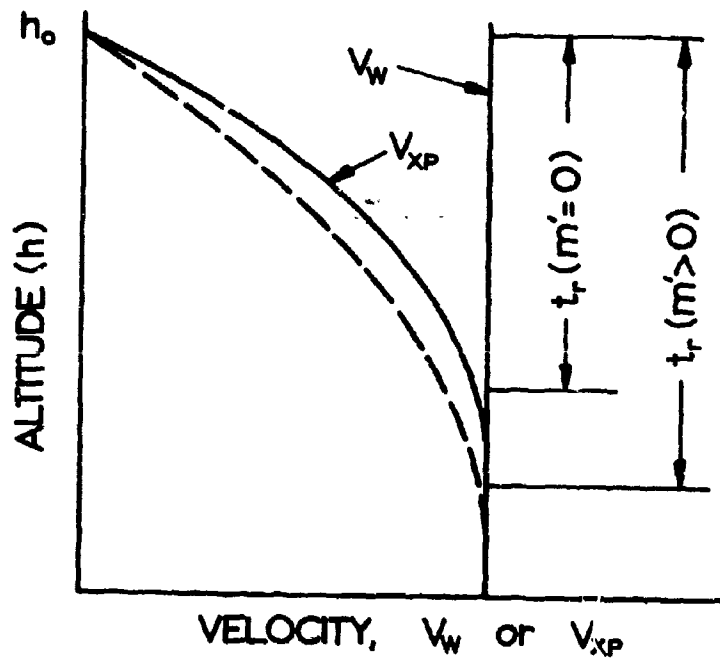
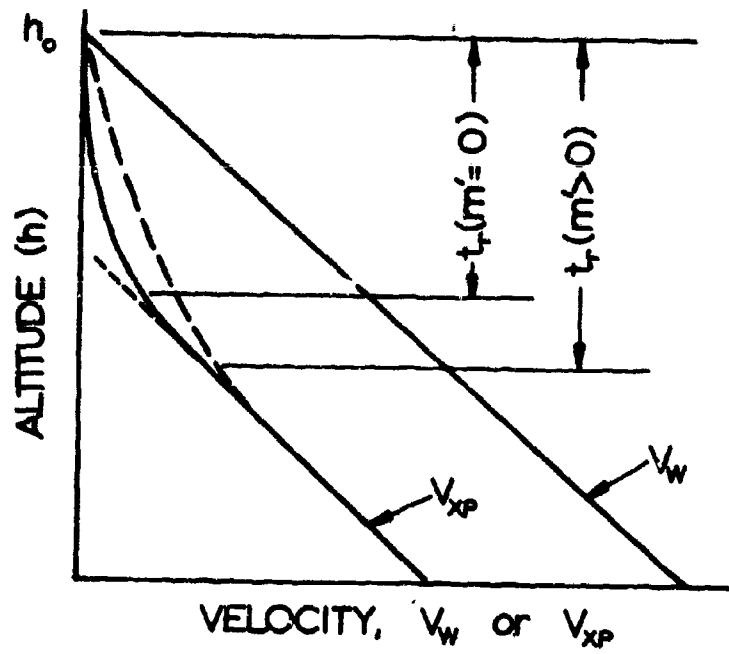


Fig 9. Effect of Apparent Mass on a Parachute's Horizontal Velocity and Response Time

B. Example Calculations

Calculations have been made for a parachute entering a wind shear layer using the results of Eqns 38, 41, 44, and 49b. The computations are based on a wind shear layer typical of those found in the atmosphere (Ref 9), which has a gradient $\gamma = 0.1$ and a maximum velocity of 40 ft/sec. A shear layer 800 ft deep, shown in Fig 10, was used together with parachute descent velocities of 25 and 50 ft/sec. The results of these calculations are cross plotted in Figs 10, 11, and 12.

Calculations have also been made for a shear layer which has a gradient $\gamma = 0.1$ and a depth of 400 ft. These computations are shown for altitude versus horizontal velocity in Fig 13, with terminal velocity conditions of 25, 50, 75, and 100 ft/sec. A set of calculations has also been completed for steady wind shear layers of 10, 20, and 40 ft/sec, shown in Figs 14, 15, and 16, respectively. In each case the terminal velocity conditions were varied from 25 to 100 ft/sec.

From the development of the preceding equations, it is evident that the particular effects of the free or damped oscillations of the parachute, which obviously are initiated when the parachute enters the shear layer, are neglected. In view of the fact that within the scope of this study, merely statically stable parachute systems are considered, and remembering that in accordance with Ref 1 the oscillations of such systems diminish very quickly, the presented method appears to be acceptable. It may also be stated that Ref 1 shows that the horizontal displacement of a statically stable system under damped oscillations is small. Therefore, the presented trajectory analysis may also be considered a good approximation, when considered from this point of view.

III. EXPERIMENTS

A. Introduction

Since the cross wind effects are of great practical importance, laboratory tests were conducted to check the validity of the analytical results. For this purpose, circular flat ribbon and ringslot models each of 15 and 25 percent total porosity and, for comparison, a ribless guide surface model with a nominal porosity of 120, were injected

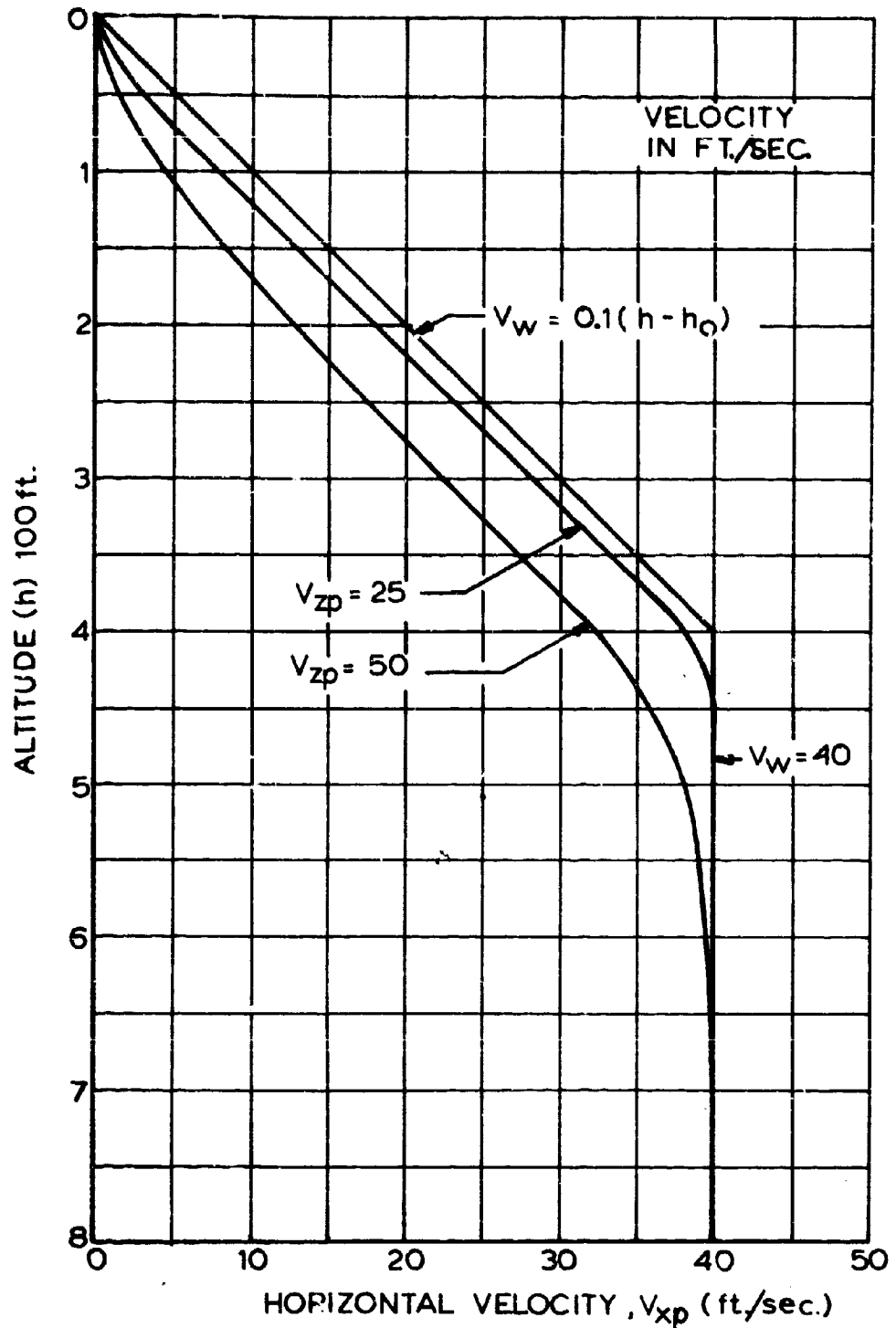


Fig 10. Horizontal Velocity as a Function of Altitude of Point-Mass Parachute System at Various Terminal Velocity Conditions, Wind Gradient (γ) = 0.1 ft/sec/ft ($0 < h < 400$), Wind Velocity (V_w) = 40 ft/sec ($400 < h < 800$)

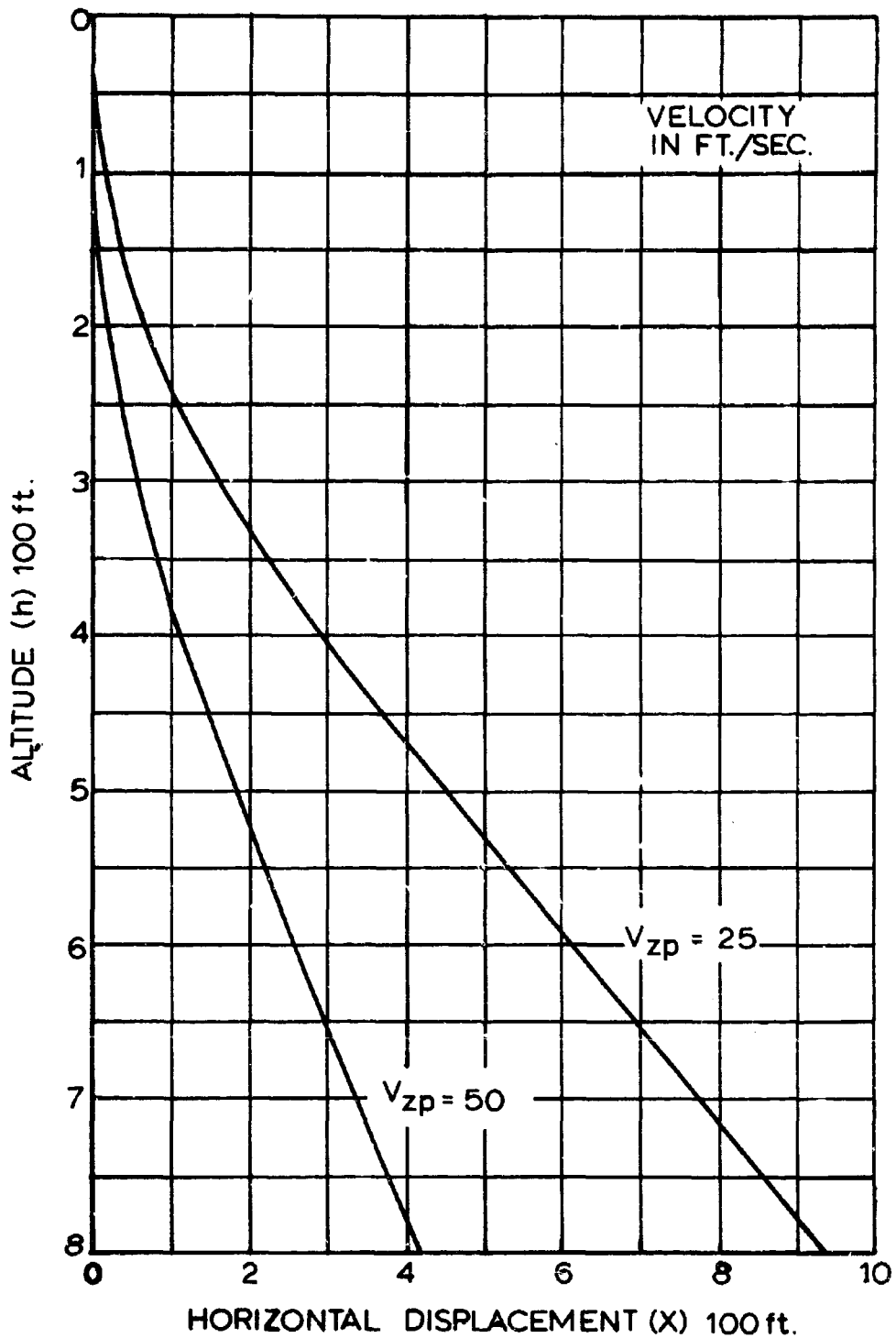


Fig 11. Trajectory for Point-Mass Parachute System at Various Terminal Velocity Conditions, Wind Gradient (γ) = 0.1 ft/sec/ft ($0 < h < 400$), Wind Velocity (V_w) = 40 ft/sec ($400 < h < 800$)

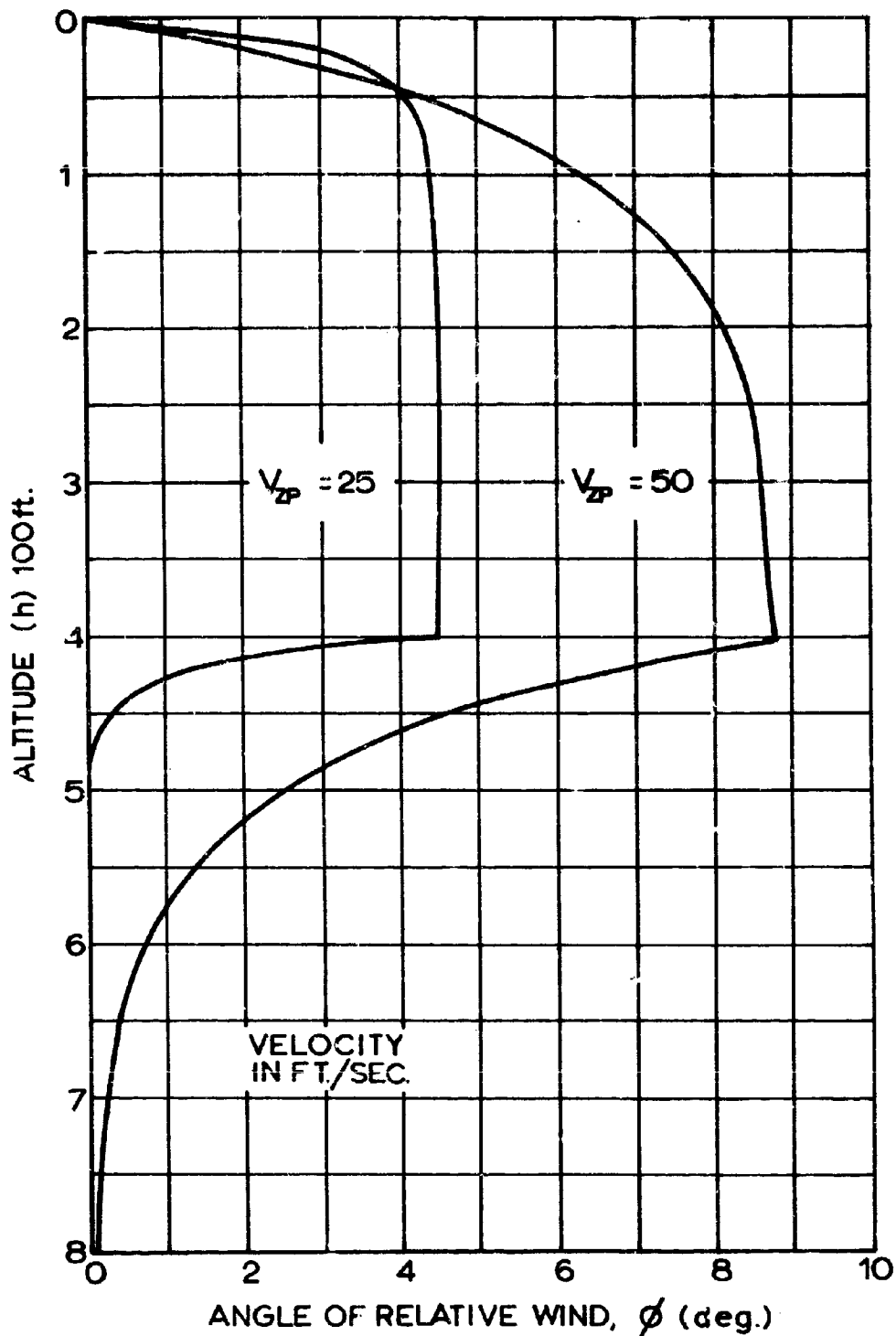


Fig 12. Angle of Relative Wind as a Function of Altitude for Point-Mass Parachute System at Various Terminal Velocity Conditions, Wind Gradient (γ) = 0.1 ft/sec/ft ($0 < h < 400$), Wind Velocity (V_w) = 40 ft/sec ($400 < h < 800$)

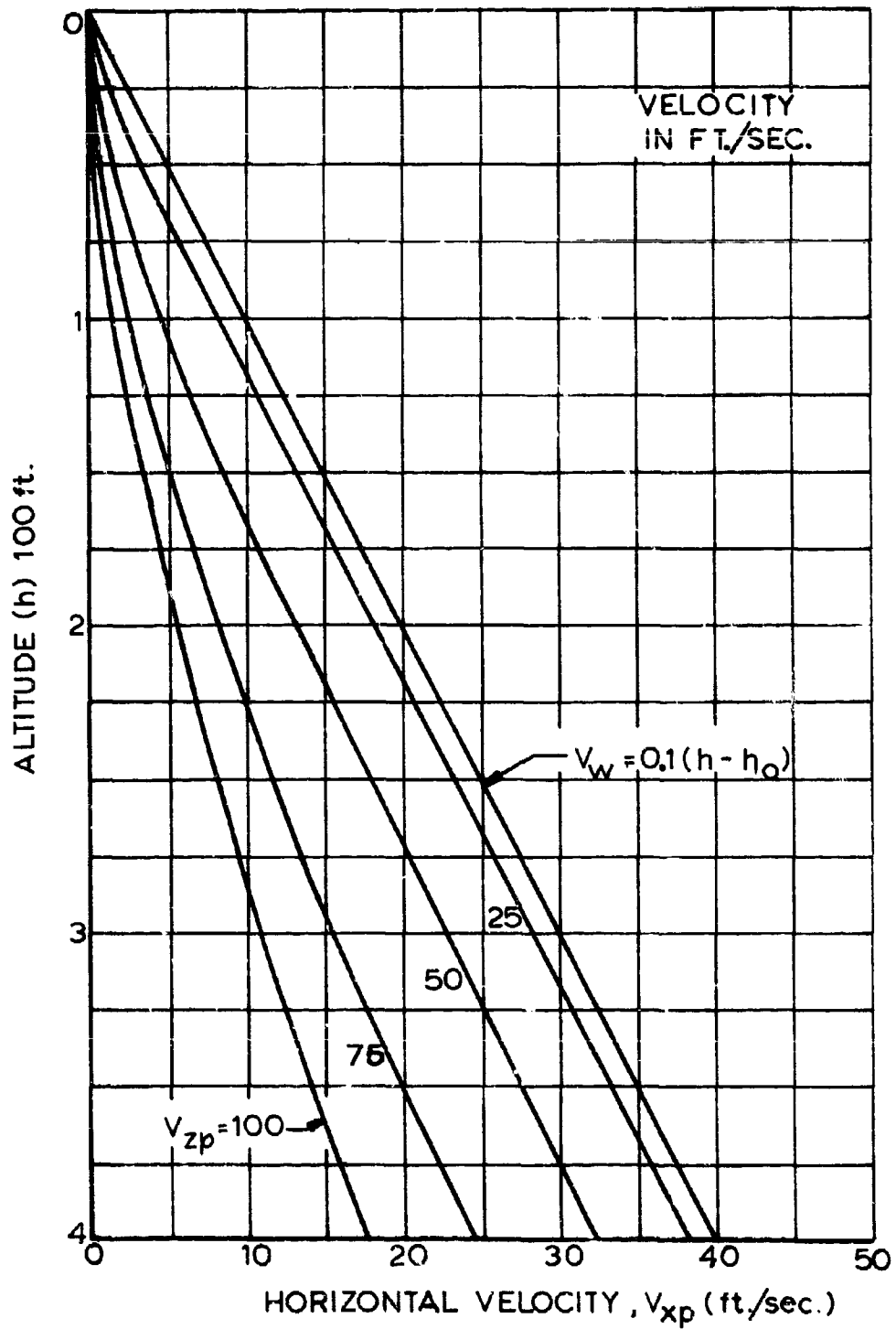


Fig 13. Horizontal Velocity as a Function of Altitude for a Point-Mass Parachute System at Various Terminal Velocity Conditions, Wind Gradient (γ) = 0.1 ft/sec/ft

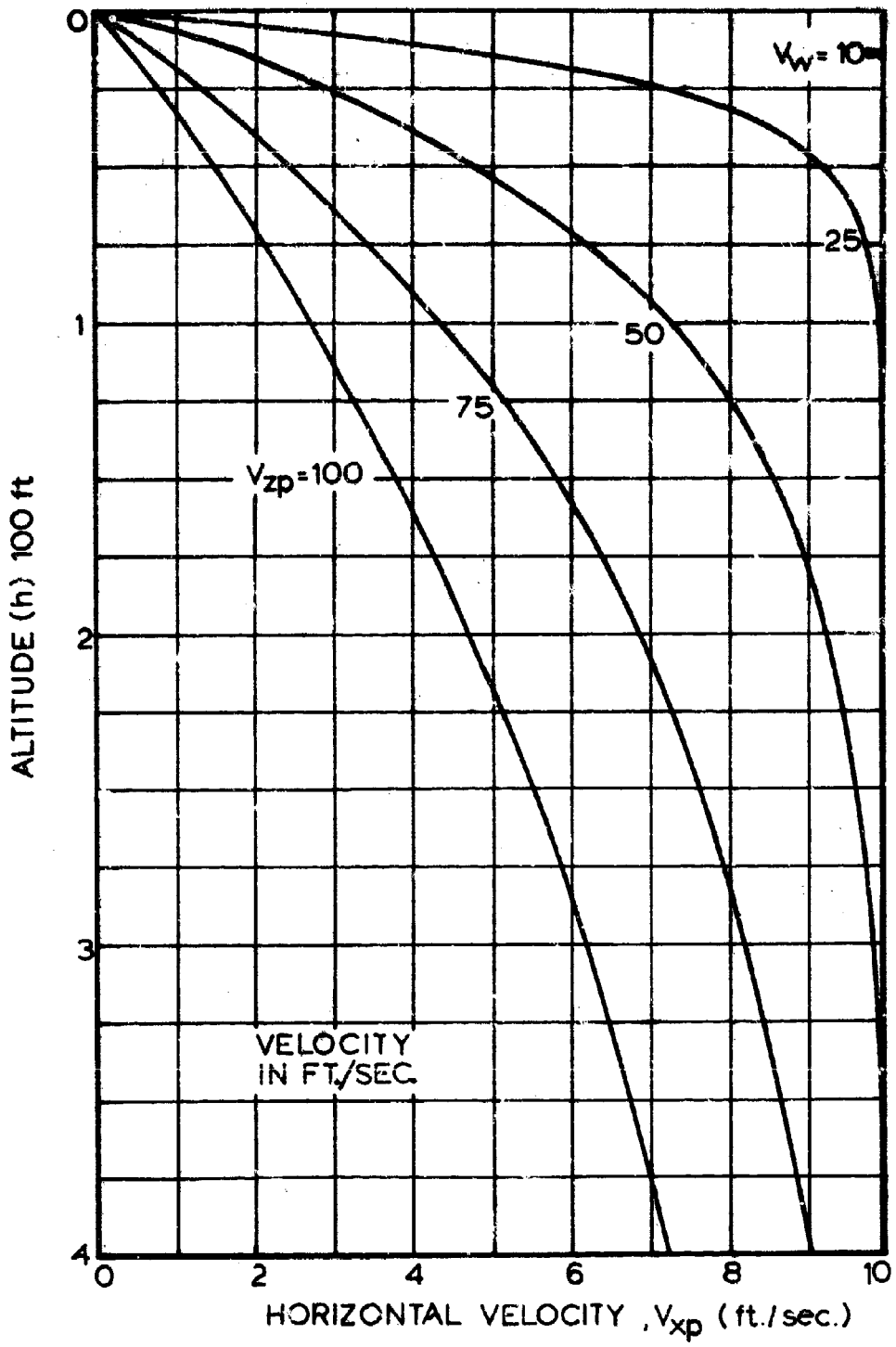


Fig 14. Horizontal Velocity as a Function of Altitude for a Point-Mass Parachute System at Various Terminal Velocity Conditions, Wind Velocity (V_w) = 10 ft/sec

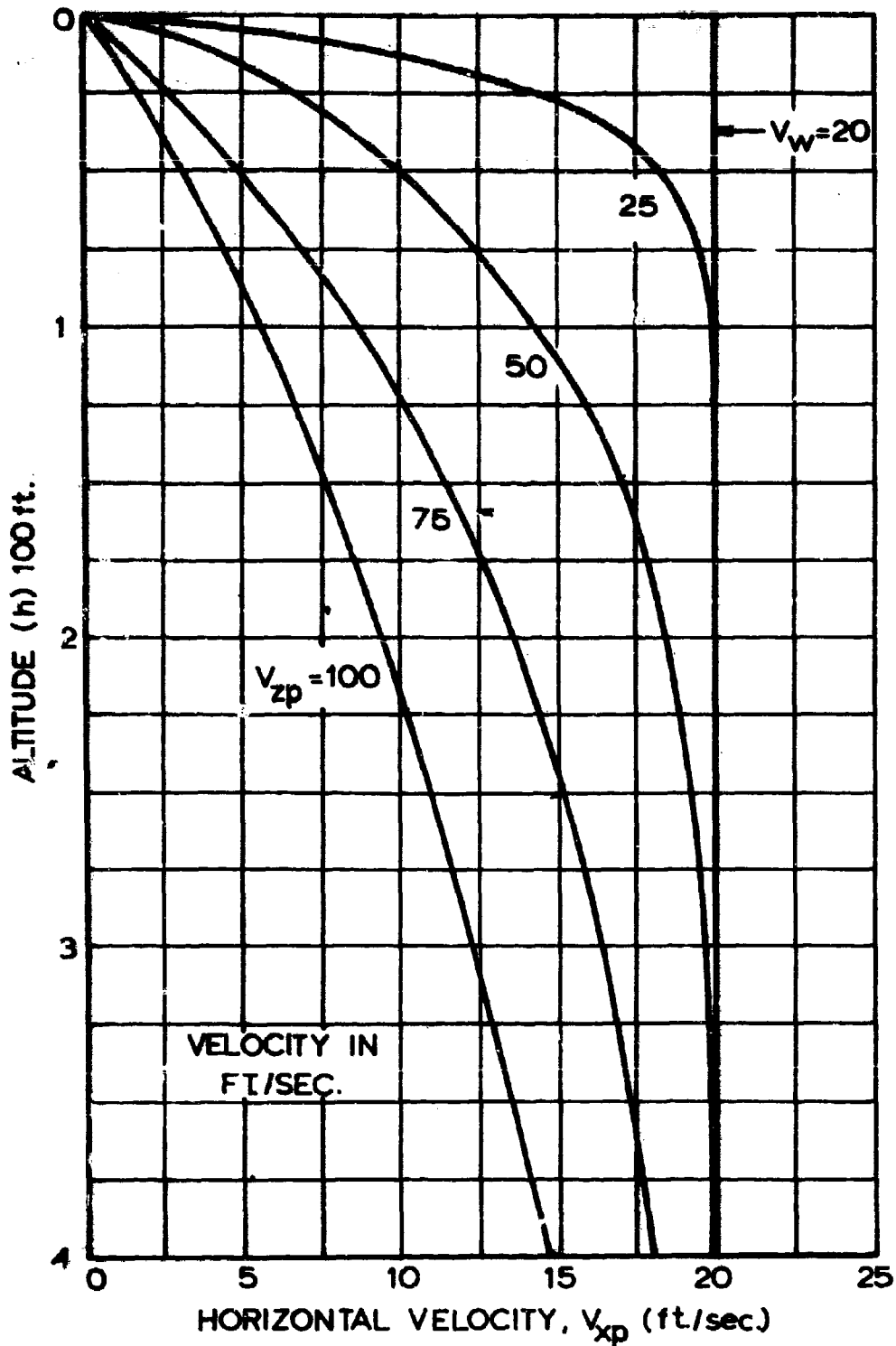


Fig 15. Horizontal Velocity as a Function of Altitude for a Point-Mass Parachute System at Various Terminal Velocity Conditions, Wind Velocity (V_w) = 20 ft/sec

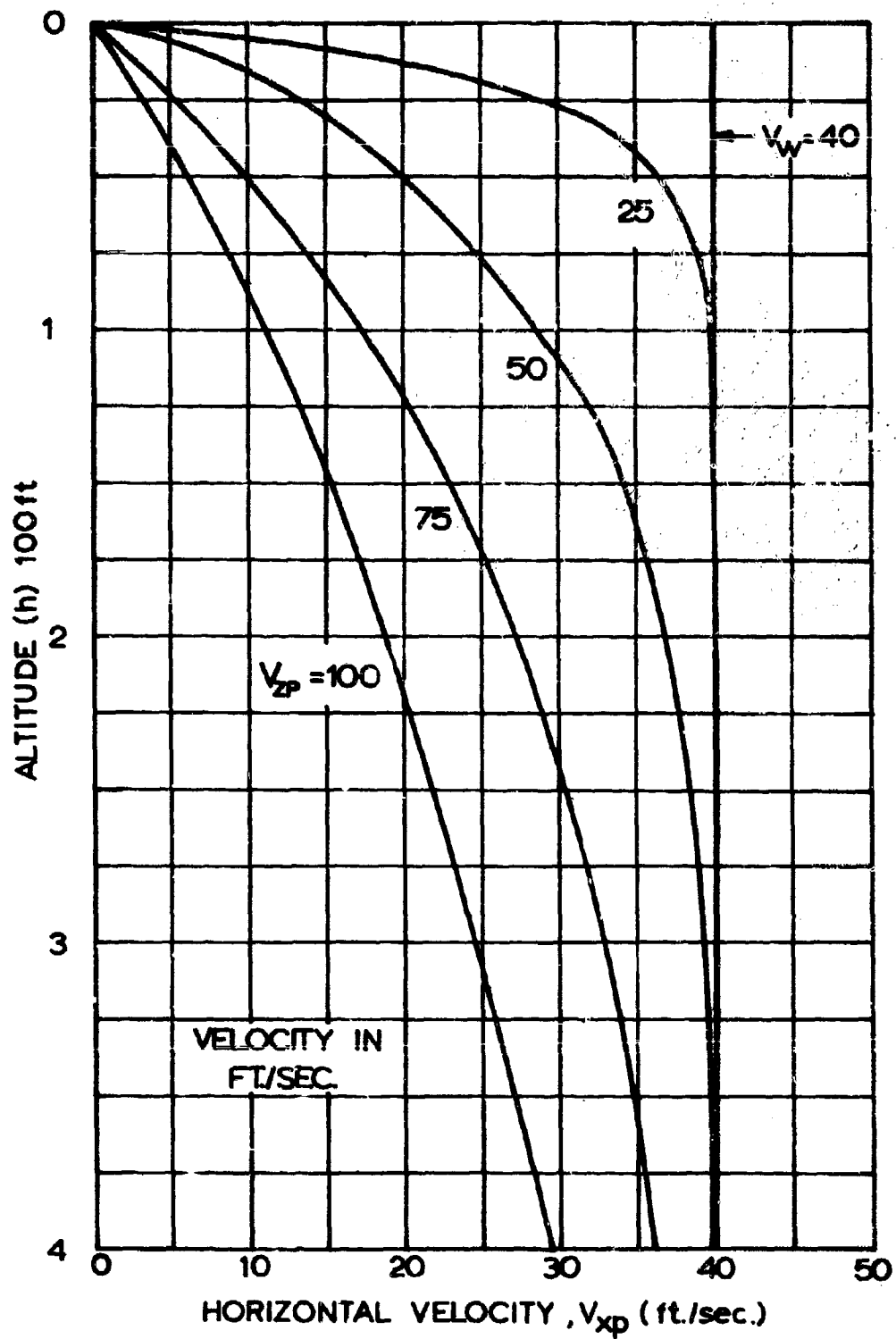


Fig 16. Horizontal Velocity as a Function of Altitude for a Point-Mass Parachute System at Various Terminal Velocity Conditions, Wind Velocity (V_w) = 40 ft/sec

into the windstream of a horizontal open test section wind tunnel. A description of the models, testing facilities, and experiments is given in Section IV.

The steady state characteristics of the parachutes used are known to be quite different (Ref 2). Hence, one would expect corresponding performance differences in the cross wind experiments.

Comparing then the results of the simplified analytical process with those of the experiments, one may observe certain characteristic differences which would be caused by the damped oscillations or the dynamic behavior of the parachute systems. Considering these deviations in view of the theory of dynamic stability, Ref 1, one may derive a refined analytical method based on the analysis given in this study, combined with certain corrections extracted from the theory of Ref 1 and from the presented experimental results. The predictions of this method would be more realistic than those available at present. Unfortunately, certain limitations prevented the accomplishment of this phase of the investigation at this time, but a qualitative comparison will be presented.

B. Experimental Procedure

The five parachute types mentioned above have been tested in both constant and varying wind fields. A steady wind tunnel speed of 37 ft/sec was used in combination with parachute terminal velocities of 20, 30, and 40 ft/sec. Experiments with terminal speeds below 20 ft/sec were found to be inconclusive because of exceptionally large angular and horizontal displacements. At speeds above 40 ft/sec the horizontal displacements were immeasurably small due to the high canopy loadings.

Varying or non-steady cross wind experiments were conducted with an established velocity gradient increasing from 5 ft/sec at the top to 45 ft/sec at the bottom of the shear layer. This wind profile corresponds to a gradient of $\delta = 5$. Attempts were made to inject models at terminal velocities of 15 and 20 ft/sec. At 20 ft/sec it was found that the thickness of the varying shear layer was insufficient to produce any measurable horizontal displacement, while at 15 ft/sec the parachute oscillations were too large to yield reliable results within the observable range. Hence, experiments with the gradient shear layer were discontinued.

C. Results

The results of experiments in the constant shear layer are presented in Figs 17 through 28 as graphs of horizontal displacement, horizontal velocity, angle of attack, and angle of relative wind as functions of the altitude. In addition to the experimental curves, a curve showing the analytical predictions is added to each figure. These analytical curves have been computed for the particular experimental conditions. The five test models are compared in each figure except for angle of attack versus time in Fig 29, which only shows oscillations of a ribless guide surface, and 15% porosity ringslot parachutes which are the most and the least stable parachute, respectively.

In detail, Figs 17, 18, and 19 represent the trajectory plots for all models at terminal speeds of 20, 30, and 40 ft/sec in a steady wind of 37 ft/sec. It can be seen that all models follow in principle the theoretical predictions. It should be realized, however, that the comparison is merely extended over the initial part of the acceleration process and one may expect a better agreement in the later portion of the trajectory.

From the trajectory curve and knowing the time at any parachute position, one can determine the horizontal parachute velocity as shown in Figs 20, 21, and 22. In each of the above figures a respective theoretical curve has been indicated.

In the case of altitude versus horizontal displacement or velocity, it appears that the high porosity parachutes, namely, the 25% porosity ringslot and ribbon, agree more closely with the theory, at least in the upper portion of the shear layer. This is due, in part, to the slow angular response of these parachutes in a cross wind and the nearly constant effective drag force of these parachutes under these stability conditions.

The angle of attack arises in view of the dynamic stability characteristics of the parachutes in free descent and is simply the difference between the parachute inclination angle and the angle of relative wind as shown in Fig 30. A statically stable parachute without dynamic effects or overshoot would always have a zero angle of attack. The investigated parachutes have different aerodynamic and dynamic characteristics and the Figs 23 through 28 indicate different angles of attack and vary in their alignment characteristics. Since the rate of descent is a consequence of the effective drag, which in turn is a function of the angle of attack, the rate of descent of the various parachutes will vary during the initial phase of the parachute alignment. Therefore, the experimental data presented in Fig 23 through 28 should also be considered in view of this aspect.

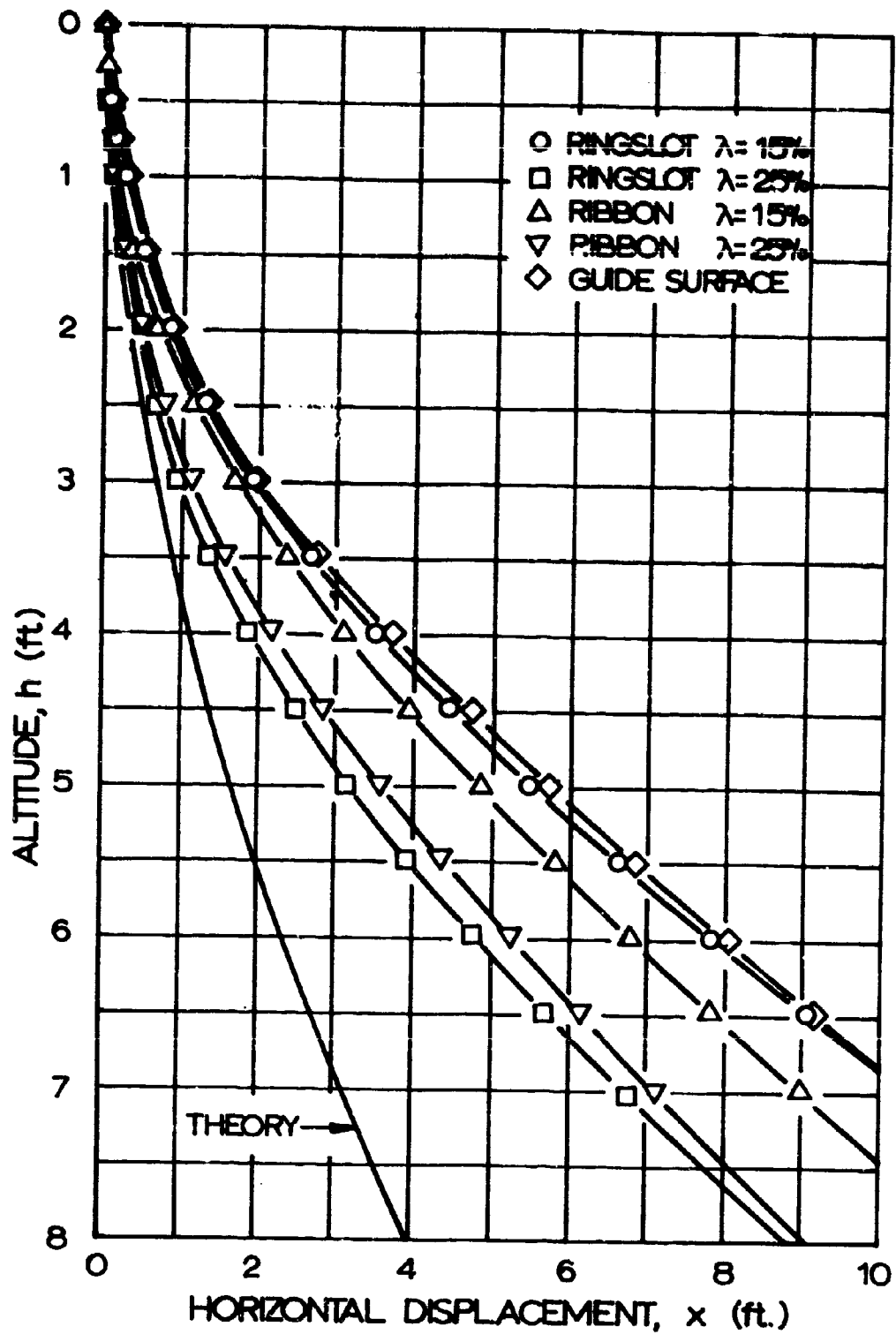


Fig 17. Trajectory of Various Parachutes, Terminal Velocity (V_{zp}) = 20 ft/sec, Wind Velocity (V_w) = 37 ft/sec

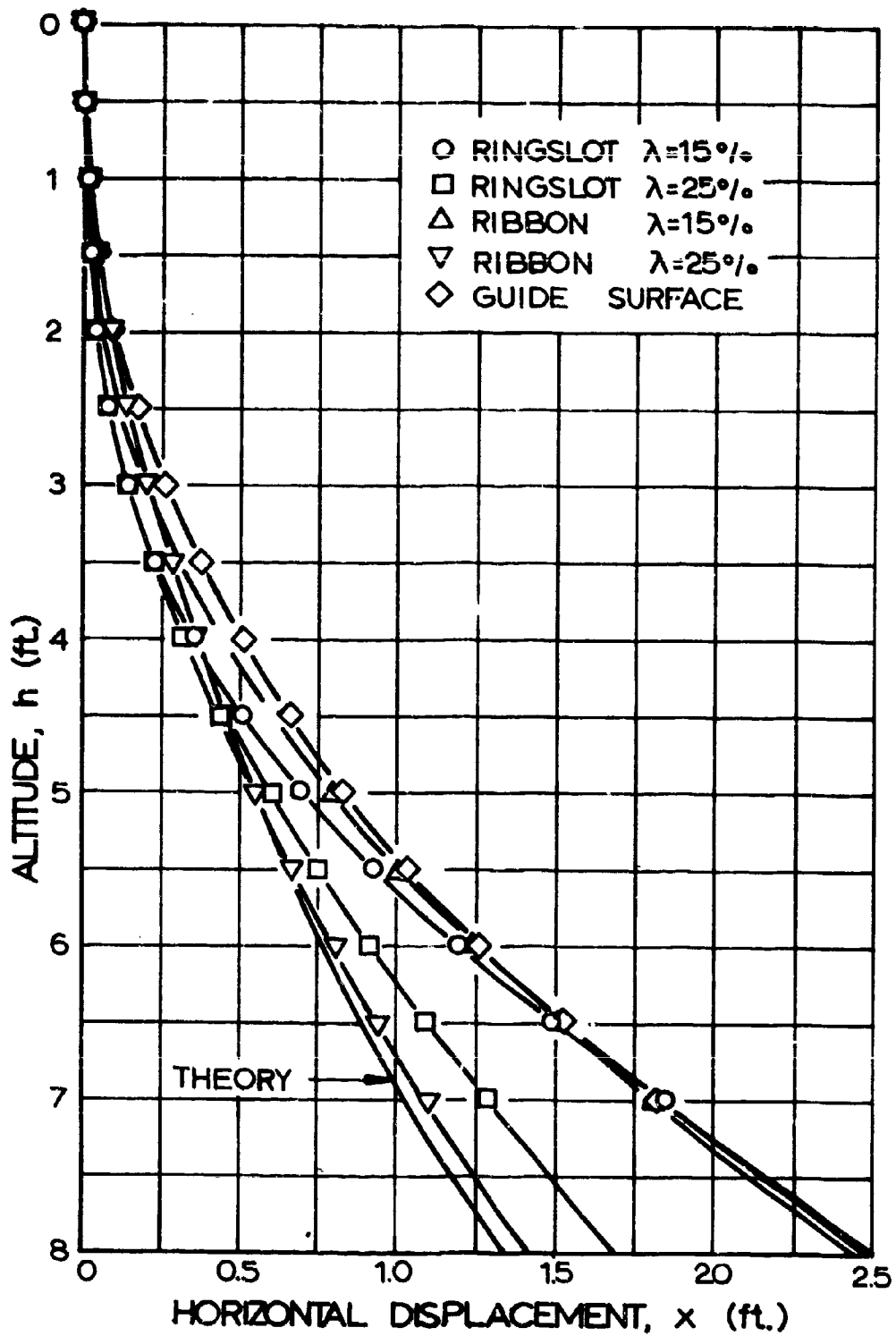


Fig 18. Trajectory of Various Parachutes, Terminal Velocity (V_{zp}) = 30 ft/sec, Wind Velocity (V_w) = 37 ft/sec

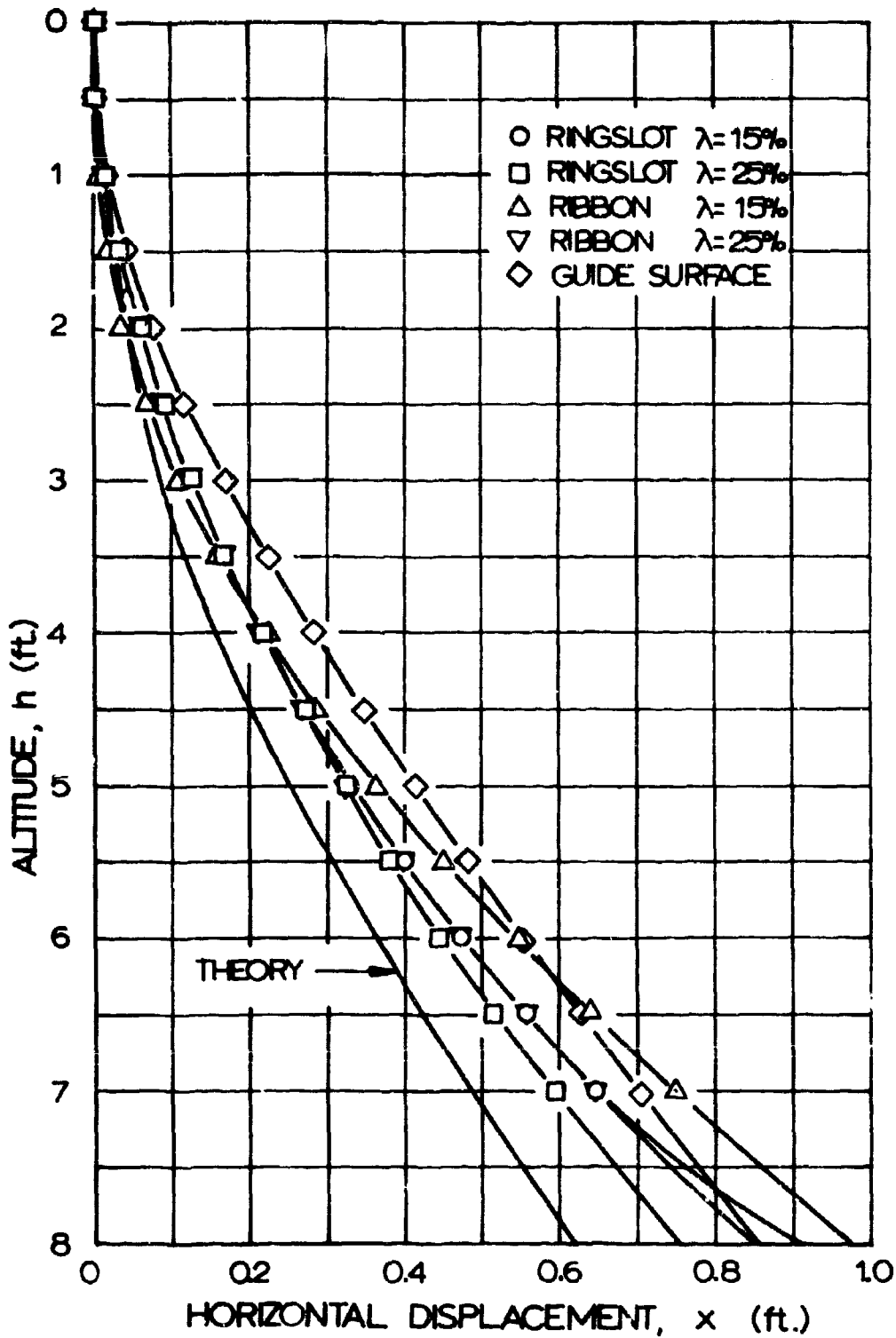


Fig 19. Trajectory of Various Parachutes, Terminal Velocity (V_{zp}) = 40 ft/sec, Wind Velocity (V_w) = 37 ft/sec

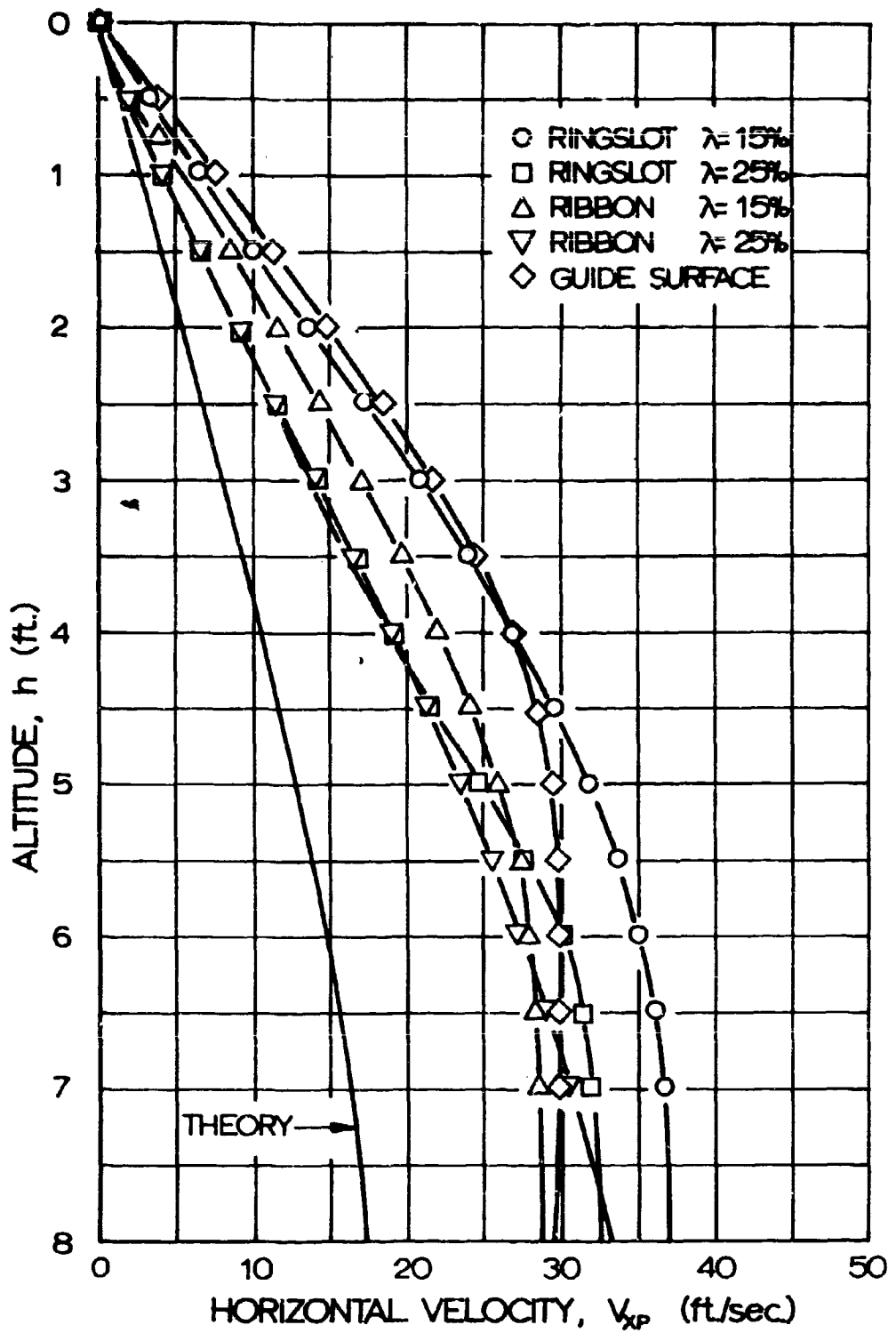


Fig 20. Horizontal Velocity as a Function of Altitude for Various Parachutes, Terminal Velocity (V_{zp}) = 20 ft/sec, Wind Velocity (V_w) = 37 ft/sec

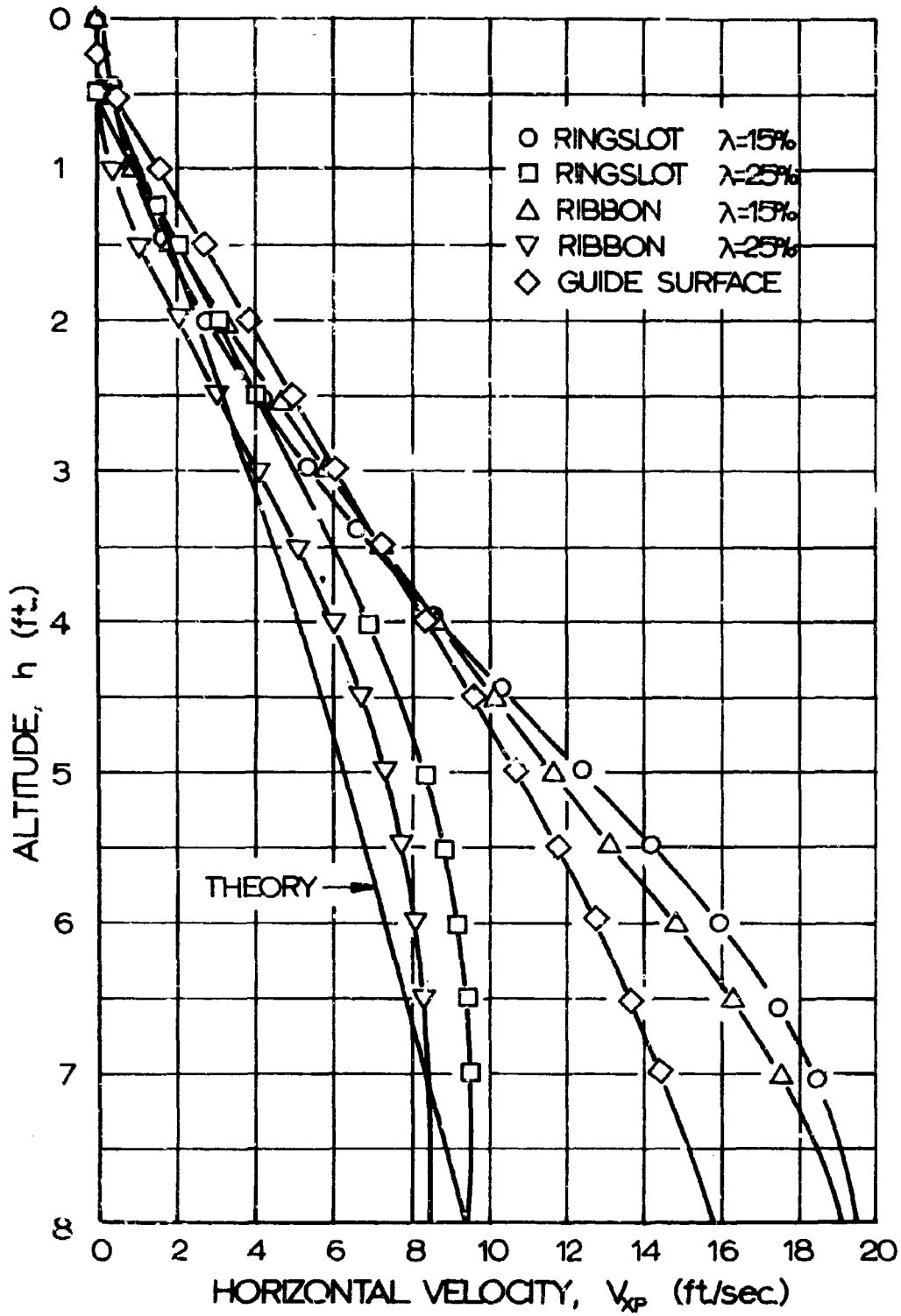


Fig 21. Horizontal Velocity as a Function of Altitude for Various Parachutes, Terminal Velocity (V_{zp}) = 30 ft/sec, Wind Velocity (V_w) = 37 ft/sec

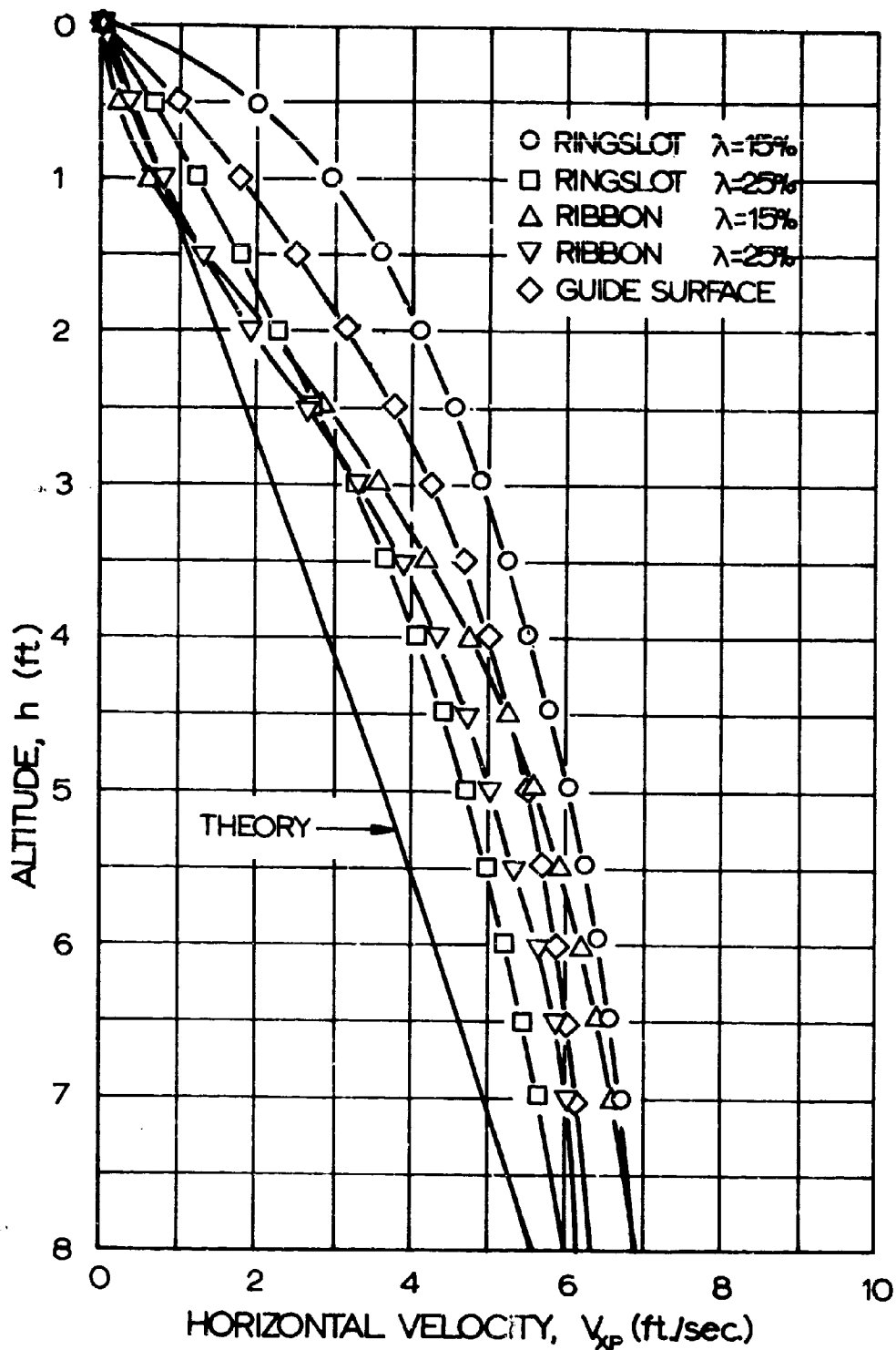


Fig 22. Horizontal Velocity as a Function of Altitude for Various Parachutes, Terminal Velocity (V_{zp}) = 40 ft/sec, Wind Velocity (V_w) = 37 ft/sec

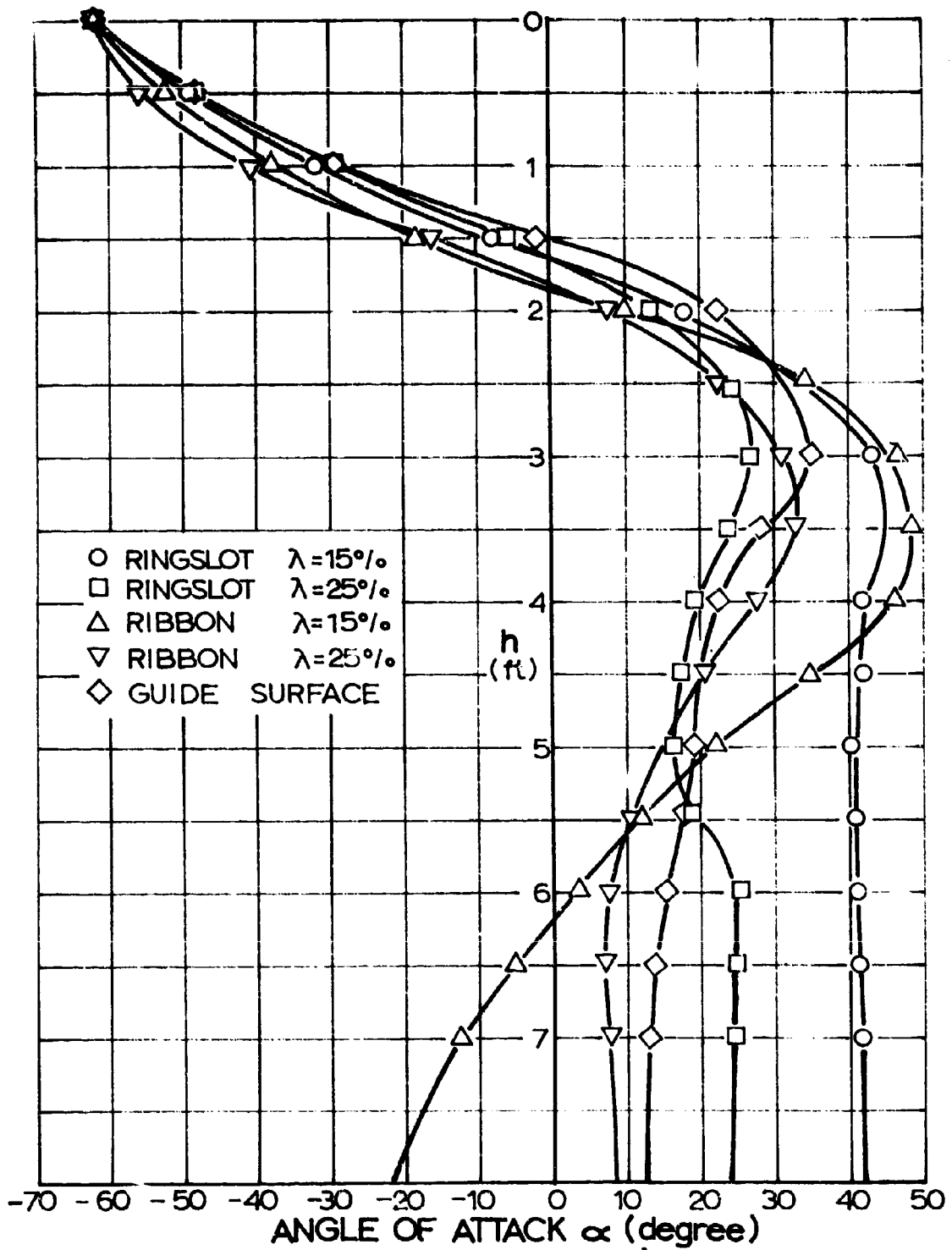


Fig 23. Angle of Attack as a Function of Altitude for Various Parachutes, Terminal Velocity (V_{zp}) = 20 ft/sec, Wind Velocity (V_w) = 37 ft/sec

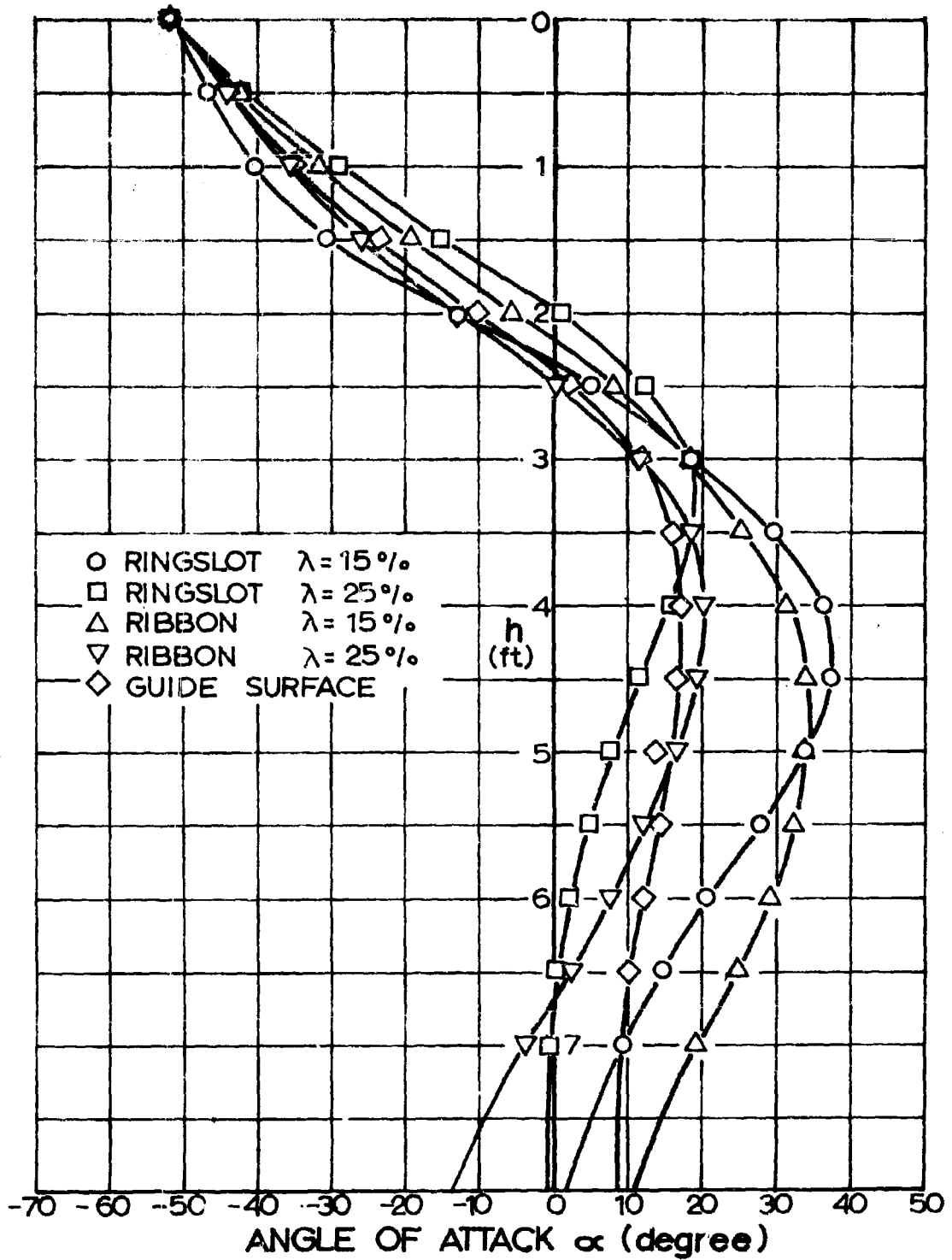


Fig 24. Angle of Attack as a Function of Altitude for Various Parachutes, Terminal Velocity (V_{zp}) = 30 ft/sec, Wind Velocity (V_w) = 37 ft/sec

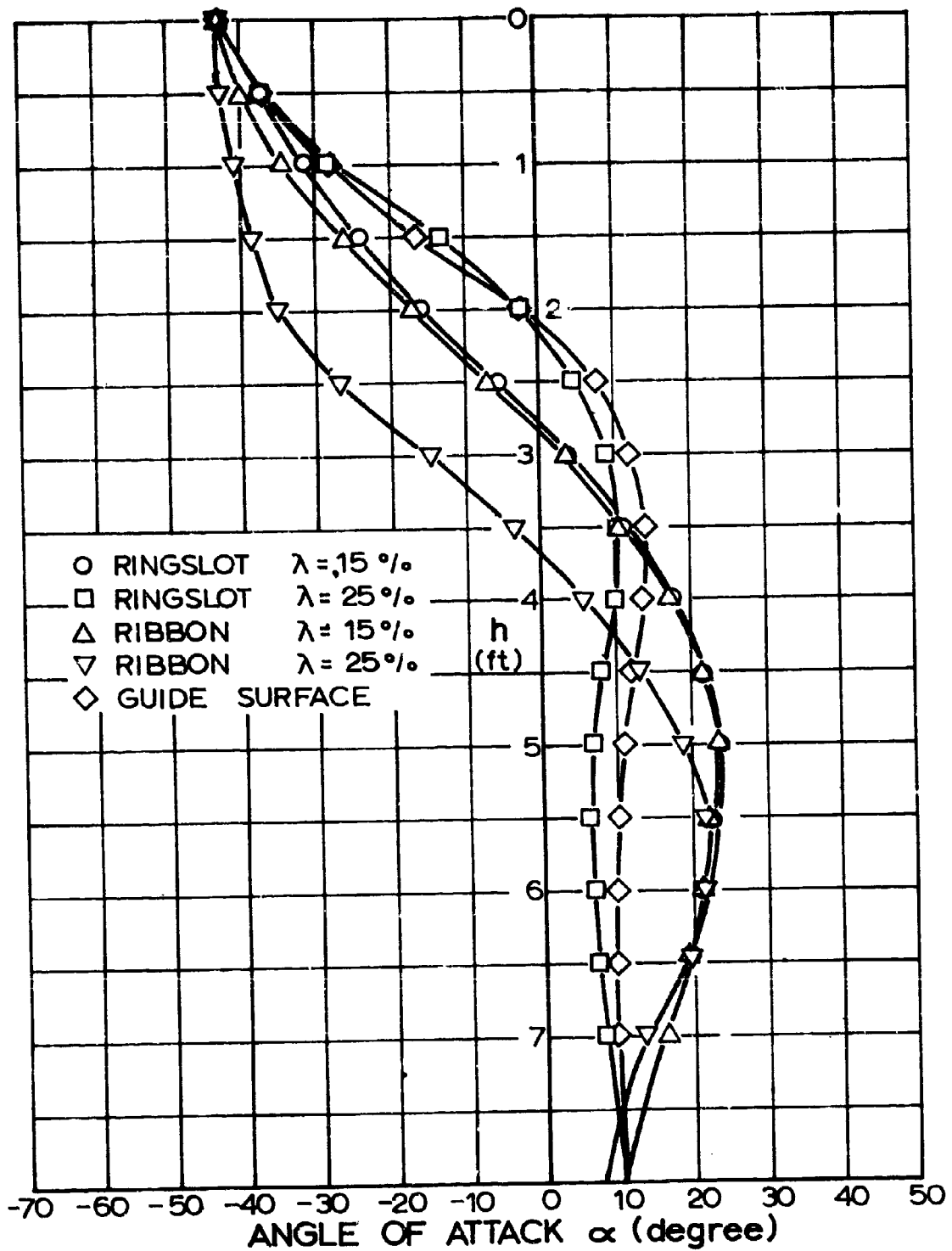


Fig 25. Angle of Attack as a Function of Altitude for Various Parachutes, Terminal Velocity (V_{zp}) = 40 ft/sec, Wind Velocity (V_w) = 37 ft/sec

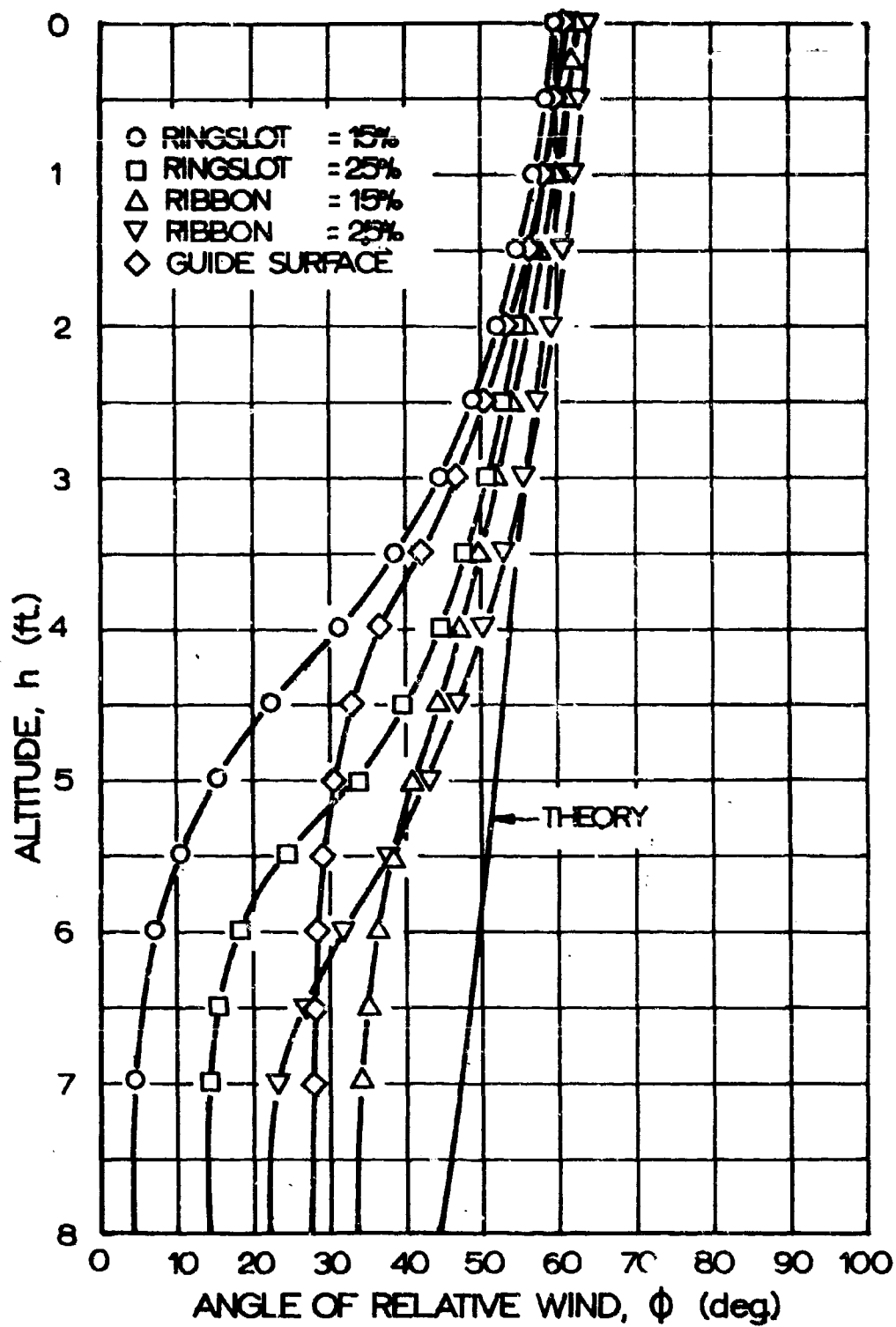


Fig 26. Angle of Relative Wind as a Function of Altitude for Various Parachutes, Terminal Velocity (V_{zp}) = 20 ft/sec, Wind Velocity (V_w) = 37 ft/sec

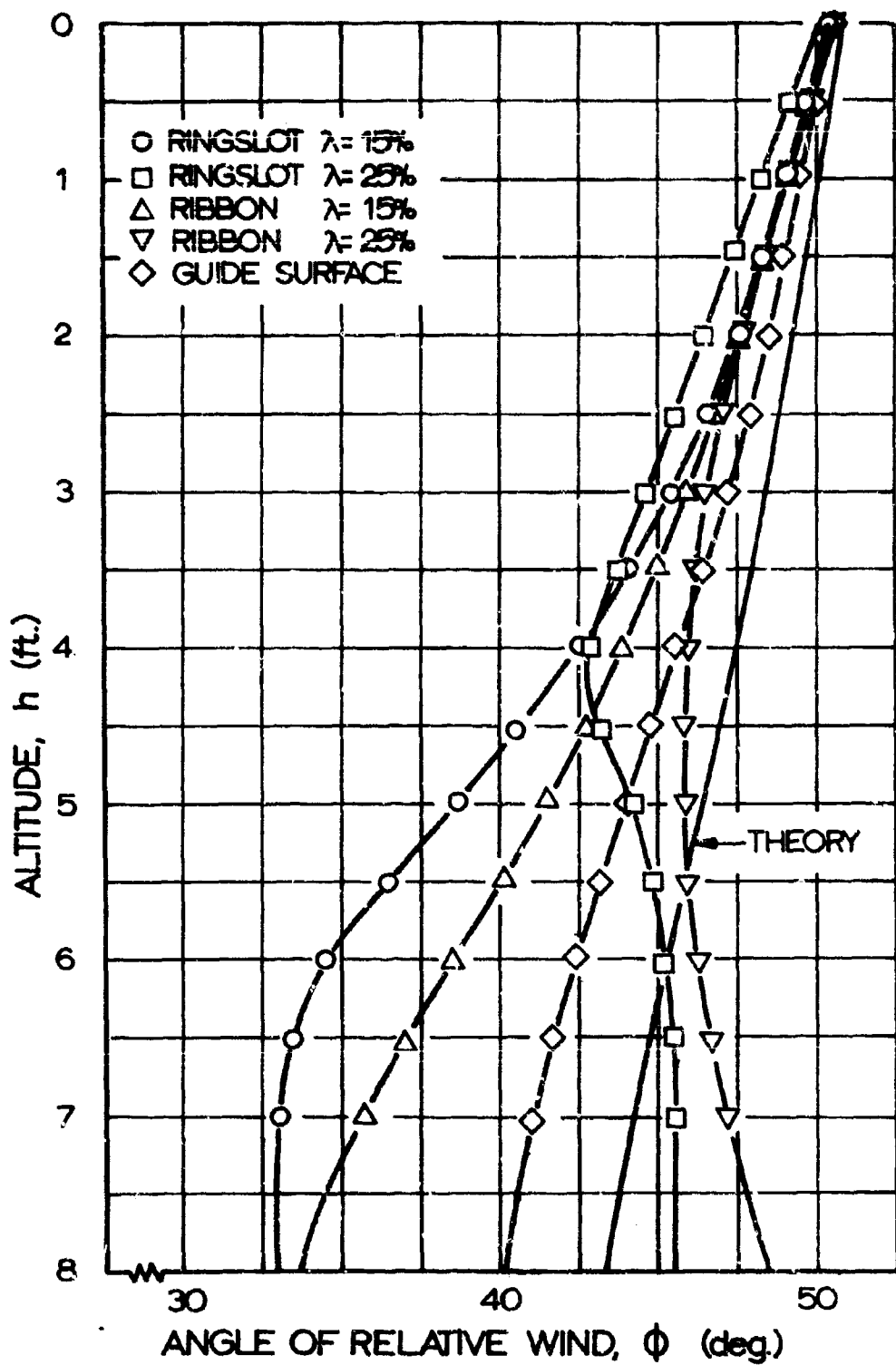


Fig 27. Angle of Relative Wind as a Function of Altitude for Various Parachutes, Terminal Velocity (V_{zp}) = 30 ft/sec, Wind Velocity (V_w) = 37 ft/sec

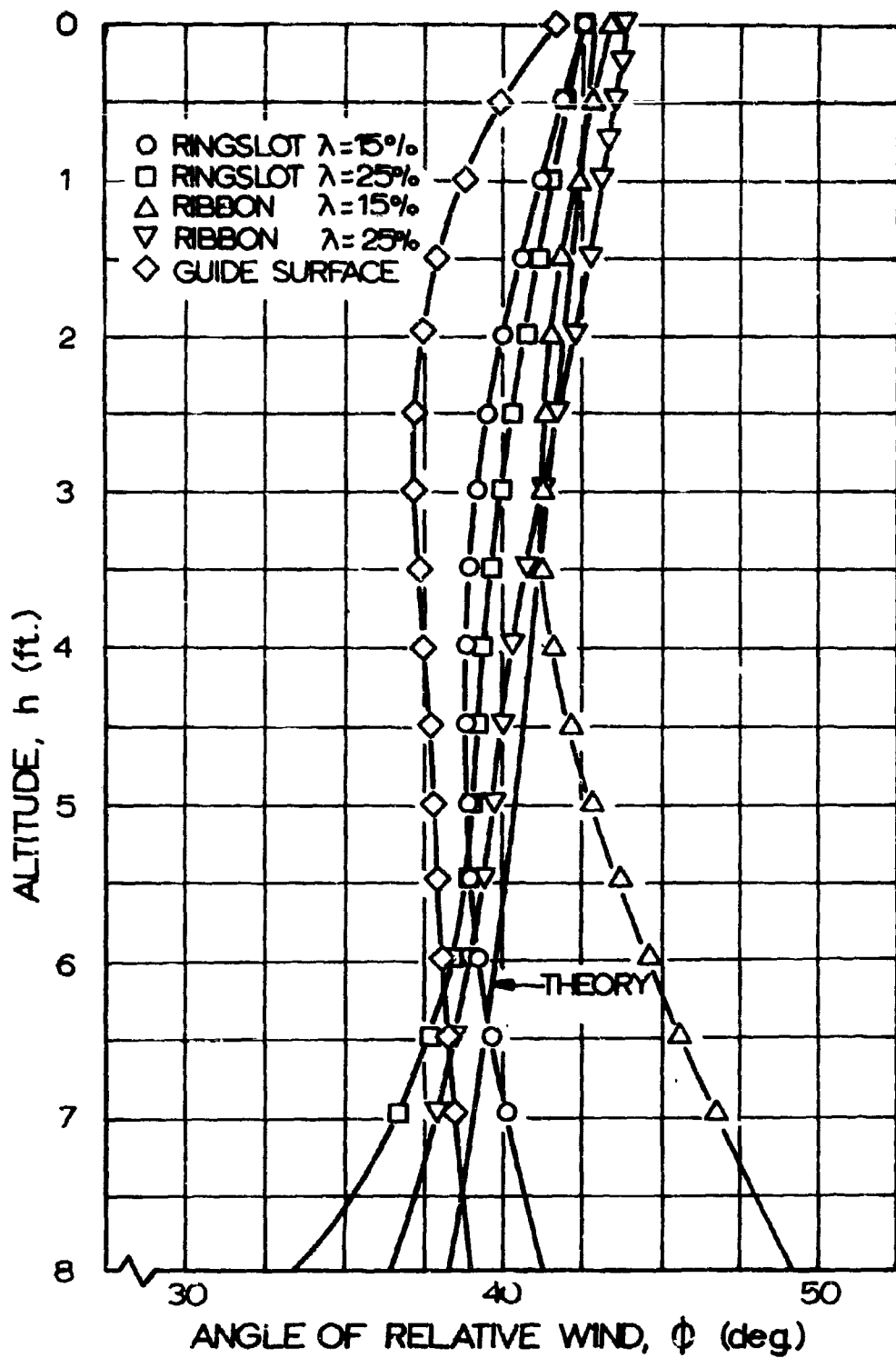


Fig 28. Angle of Relative Wind as a Function of Altitude for Various Parachutes, Terminal Velocity (V_{zp}) = 40 ft/sec, Wind Velocity (V_w) = 37 ft/sec

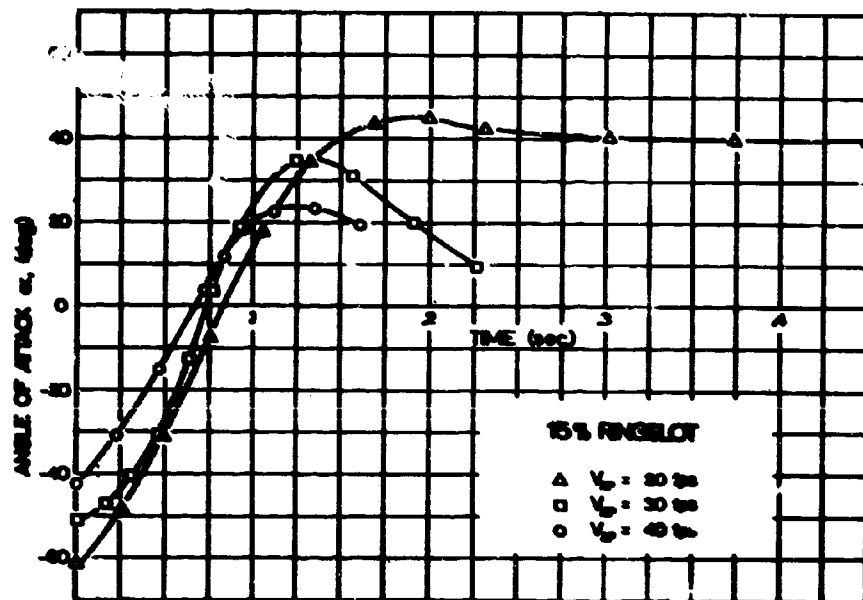
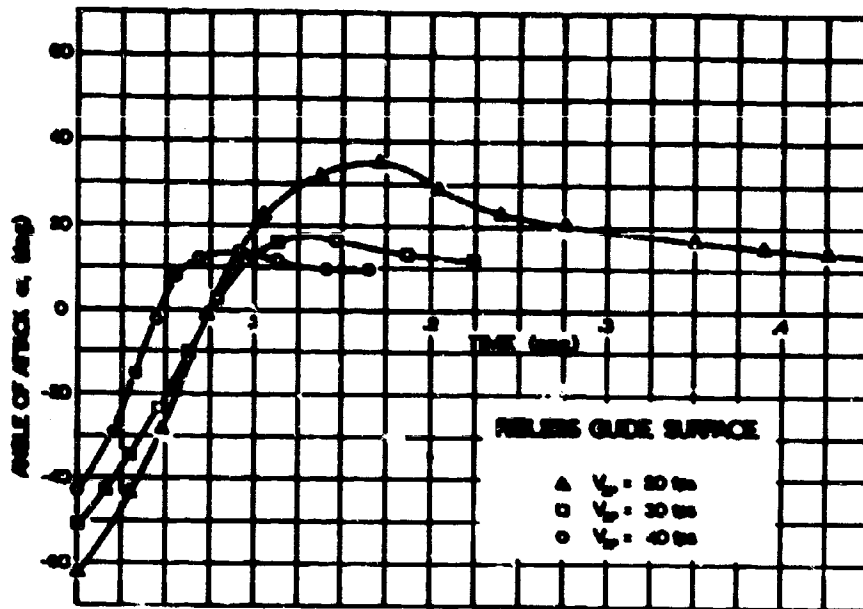
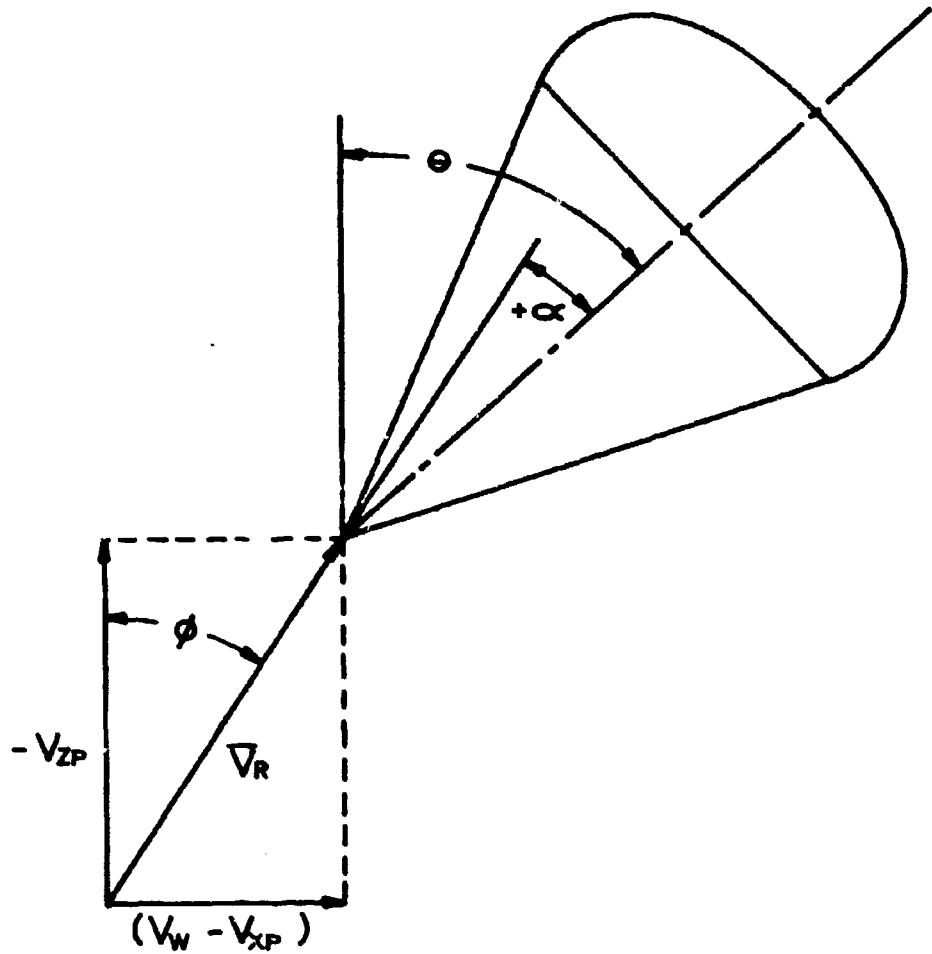


Fig 29. Angle of Attack as a Function of Time for the Ribless Guide Surface and 15% Ringslot Parachute at Various Terminal Velocity Conditions, Wind Velocity (V_w) = 37 ft/sec



- Parachute Inclination Angle
- φ Angle of Relative Wind
- α Angle of Attack ($\theta - \phi$)

Fig 30. Orientation of Parachute and Relative Wind Vector in Experiments

In general, the results indicate that, as the terminal velocity of the parachutes is increased, the experimental observations agree more closely with the simplified theory as formulated in Section II. Figures 23, 24, and 25 illustrate that, in general, the angle of attack caused by the parachute oscillation is greater at low terminal velocities than at high terminal velocities. The oscillation is first exhibited when the canopy enters the shear layer. This side gust causes an angular motion which is a series of damped oscillations. In these experiments the observable process was about one half cycle because of the small shear layer involved.

The restoring moment of each canopy will determine the magnitude of these oscillations and the rate of damping. Hence, one would expect a highly stable and well damped canopy to exhibit less oscillations than other parachutes. As an example, the ribless guide surface parachute is compared with the 15% porosity ringslot in Fig 29. It is apparent that the ribless guide surface dampens faster than the ringslot, as would be expected. This effect is due to the damping characteristics, which are related to the stability derivative $dC_m/d\alpha$. Reference 2 indicates that the ribless guide surface is statically more stable than the ringslot parachute and the observed dynamic behavior is probably a consequence of the stronger stability derivative.

It is also evident that in principle both of the highly stable parachutes, namely the 25% ribbon and the guide surface parachutes, approach in any case the theoretical angle of relative wind closer than the less stable parachutes.

A further observation is interesting to note. Namely, when the parachutes operate at a positive angle of attack, they present a larger drag area to the horizontal wind. Thus, one would expect that the models would be accelerated more rapidly than predicted by theoretical considerations, which operate with a constant drag area. This effect is evident in the trajectory and velocity plots. Therefore, the experiments have been conducted under conditions which do not fully satisfy the assumptions made in the analysis, which assumed as a basic condition that the parachute aligned itself with the relative wind instantaneously to a zero angle of attack.

The experiments show that, with higher terminal speeds of the parachutes, the initial angle of attack is decreased and the experimental results agree more closely with theory. Furthermore, it can be seen that the most stable parachutes align themselves faster to the resulting velocity, and the angle of attack approaches zero relatively

fast. This experience shows that the more stable parachutes follow in this respect the theoretical predictions best. Both observations tend to support the theoretical findings and the validity of the analytical approach.

D. Conclusions

The behavior of steadily descending parachutes under cross wind influence has been analyzed on the basis of a simplified equation of motion. A number of predictions concerning horizontal displacement, resultant velocity, and angle of deflection have been made.

Experiments were conducted which showed, in general, agreement with the theoretical predictions of horizontal displacement and velocity. Particularly good agreements were observed with the high porosity ribbon and ringslot parachutes as they initially enter the shear layer.

It was also found that the highly stable parachutes, namely the ribless guide surface, high porosity ribbon, and ringslot canopies align themselves fastest to the relative wind and assume fastest the horizontal wind velocity. In practice, their oscillations would dampen out fastest.

These statements, however, should be understood to be valid for the range of the investigation performed under this study. Speculatively, it may be said that in the later portion of the trajectories, all statically stable parachutes will align themselves closely to the theoretical curves.

IV. EXPERIMENTAL APPARATUS AND PROCEDURE

A. Introduction

The experimental equipment needed for the study of cross wind effects posed some unusual requirements, and a particular design with various engineering compromises became necessary.

B. Models

Five parachute models were used in the cross wind effects program, including circular flat ribbon and ringslot canopies each of 15 and 25 percent total geometric porosity

and a 120 nominal porosity ribless guide surface parachute. Photographs and gore patterns for these canopies are shown in Figs 31 through 34.

All ribbon and ringslot parachutes were constructed with a nominal diameter of 16 inches, while the ribless guide surface had a 12.6 inch design diameter. The ribbon and ringslot parachutes had 28 gores and suspension lines and the ribless guide surface had only 12 gores and suspension lines. Significant dimensions of each model are given in Figs 32 and 34.

The canopy sizes were selected in view of difficulties involved with the fabrication of small canopies. Generally, parachute models with nominal diameters less than 16 inches are difficult to construct and still maintain reasonable aerodynamic characteristics.

C. Cross Wind Tunnel

Considering the minimum size parachute models to be employed, an open jet wind tunnel with an 8 ft high, 3.5 ft wide nozzle was designed. This insured that the parachutes would stay in the wind field during their descent. The 8 ft high nozzle would also give the model sufficient vertical distance to respond to the cross wind.

Aerodynamically, the wind tunnel configuration was based on experiments made with a 1/12 scale model tunnel which particularly was used to study means of producing gradient wind profiles. Basically, the wind tunnel consists of three sections, namely the nozzle, diffuser, and fan, as shown schematically in Fig 35.

The nozzle section (Fig 36) has a contraction ratio of 2.3 to 1. Horizontal shelves at the mouth of the nozzle serve to straighten the flow after it passes over the turning vanes. Using these turning vanes, it is possible to maintain a velocity gradient at the nozzle exit. Figure 37 shows how the constant wind and gradient wind profiles were obtained using the turning vanes.

A diffuser was added ahead of the nozzle to steady the flow after leaving the fan. This section is essentially 8 ft square and 24 ft long. For simplicity, the section was made with straight walls except near the fan, where a transition faring was fitted to the fan.

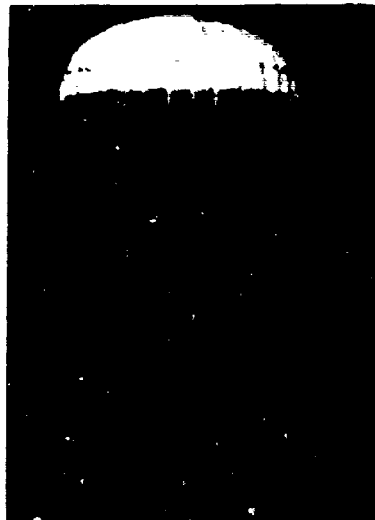
The wind tunnel was to provide a 40 ft/sec constant wind corresponding to a flow rate of 70,000 CFM. In view of this requirement, a tubular-centrifugal fan was purchased from American Standard Corporation and coupled to a 40 hp motor. Adjustable inlet vanes on the fan allowed the flow



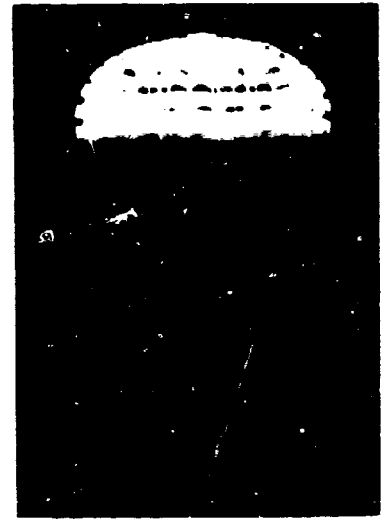
RIBBON PARACHUTE
28 GORE $\lambda=15\%$



RIBBON PARACHUTE
28 GORE $\lambda=25\%$



RINGSLOT PARACHUTE
28 GORE $\lambda=15\%$



RINGSLOT PARACHUTE
28 GORE $\lambda=25\%$

Fig 31. Circular Flat Ribbon and Ringslot Parachute Models

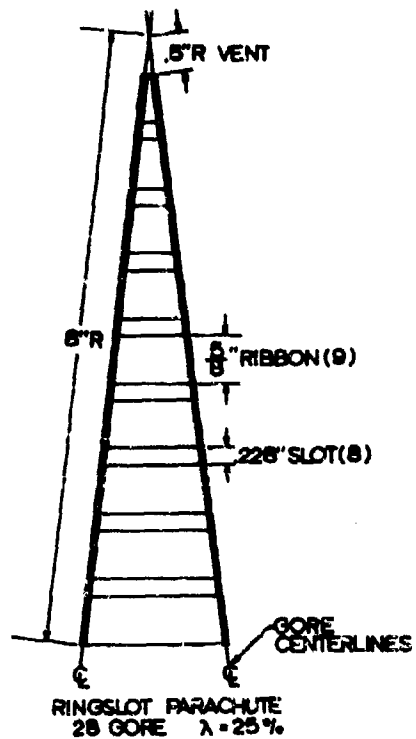
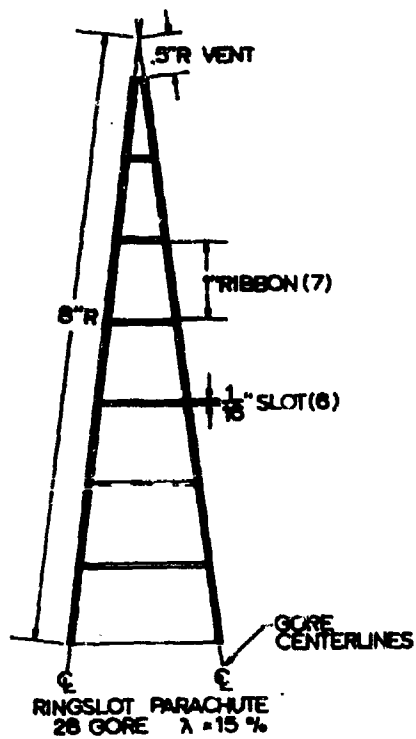
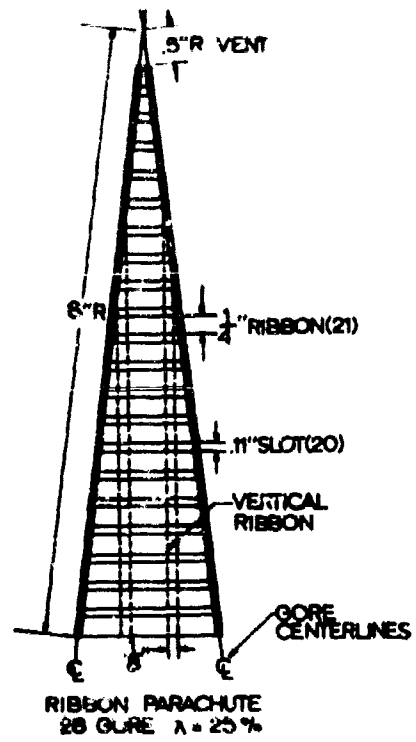
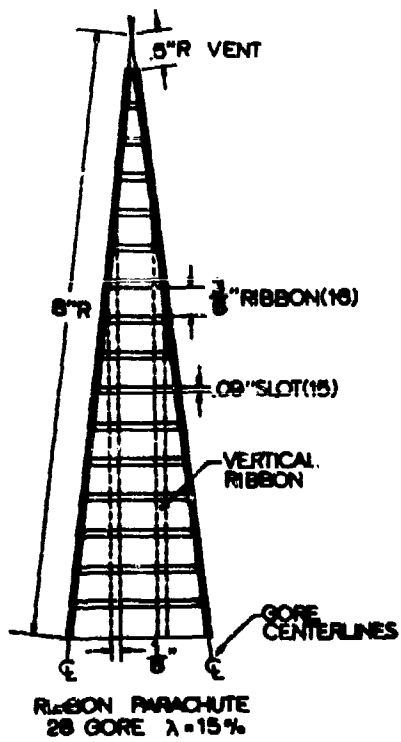


Fig 32. Gore Patterns for Circular Flat Ribbon and Ringslot Parachute Models

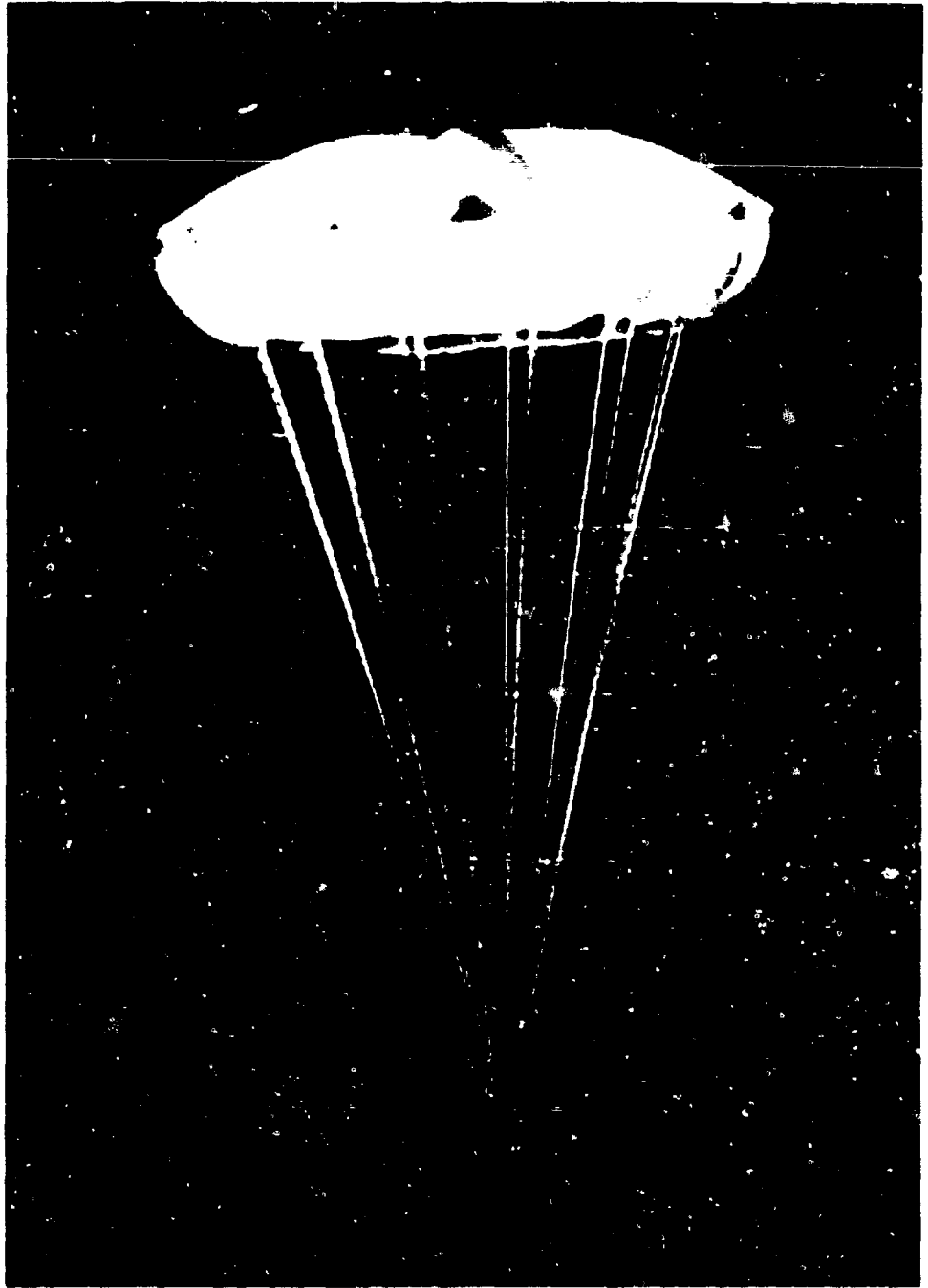
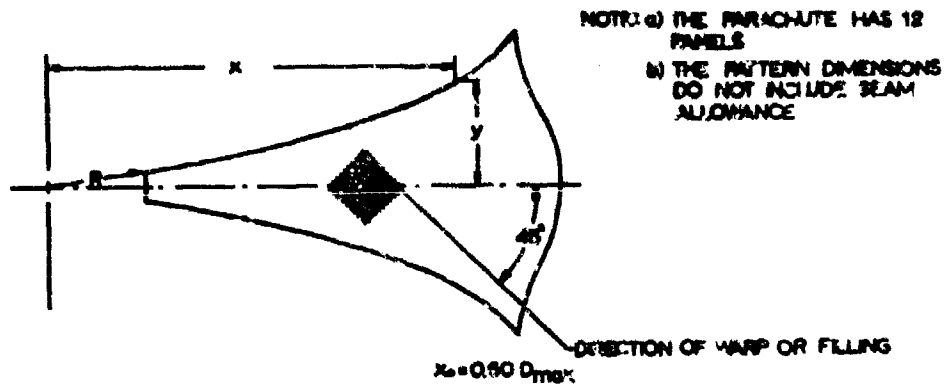
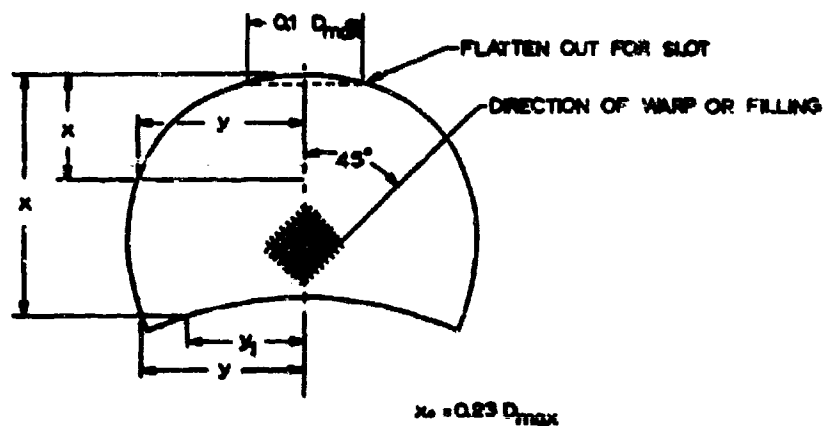


Fig 33. Ribless Guide Surface Parachute Model



x/x_0	0.10	0.20	0.30	0.40	0.50	0.60	0.70	0.80	0.875	0.90	0.95	0.975	1.0
y/x	0.394	0.364	0.394	0.407	0.410	0.416	0.428	0.441	0.485	0.527	0.581	0.625	0.0

Roof Pattern



x/x_0	0.05	0.10	0.15	0.20	0.30	0.40	0.50	0.60	0.70	0.80	0.90	0.93	0.95	1.00
y/x	4.33	3.21	2.56	2.13	1.58	1.25	1.03	0.86	0.722	0.61	0.515	0.491	0.472	0.430

Guide Surface Pattern

Fig 34. Gore Patterns for Ribless Guide Surface Parachute Model

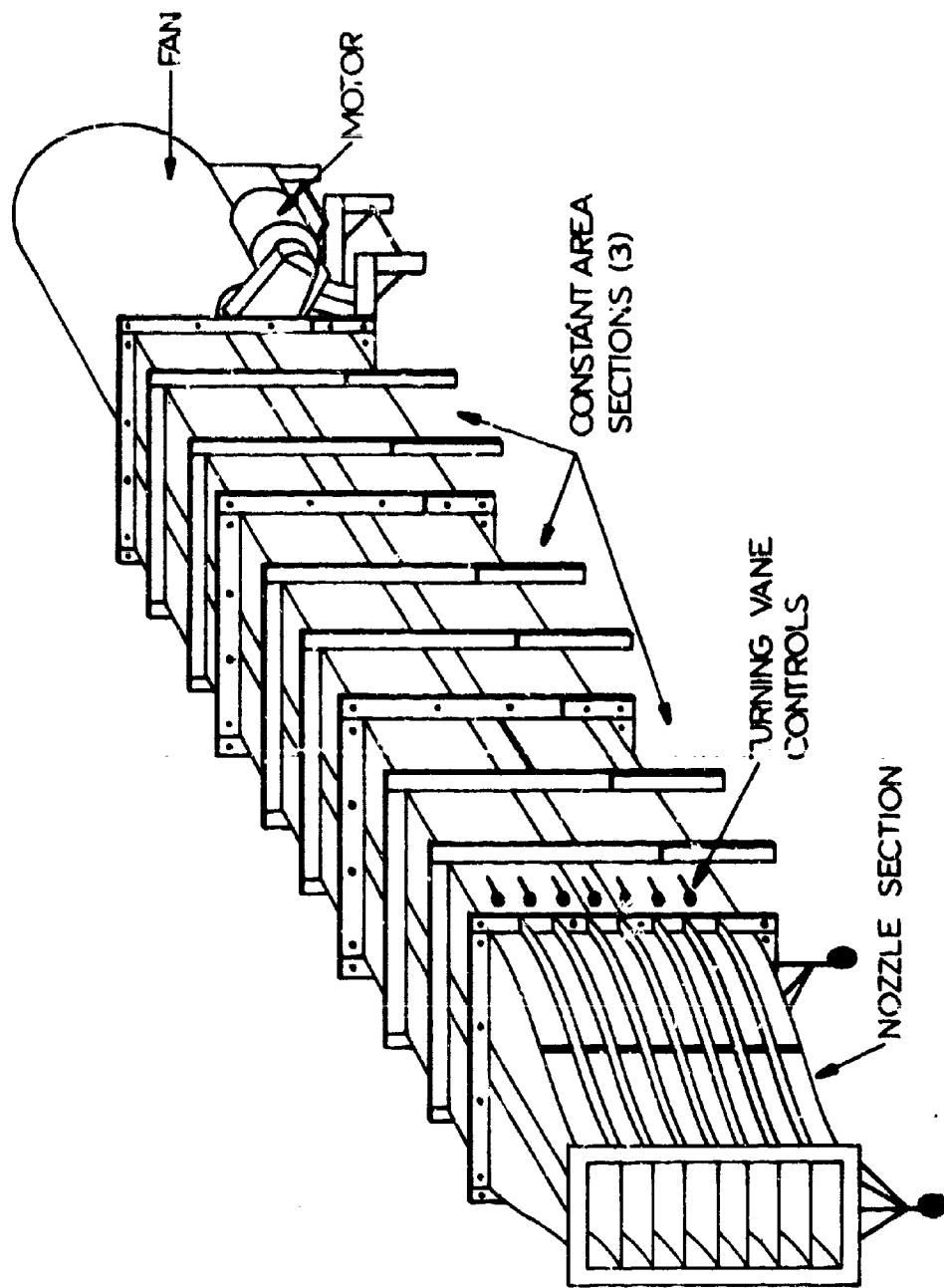


Fig 35. Cross Wind Tunnel



Fig 36. Nozzle Section of Cross Wind Tunnel

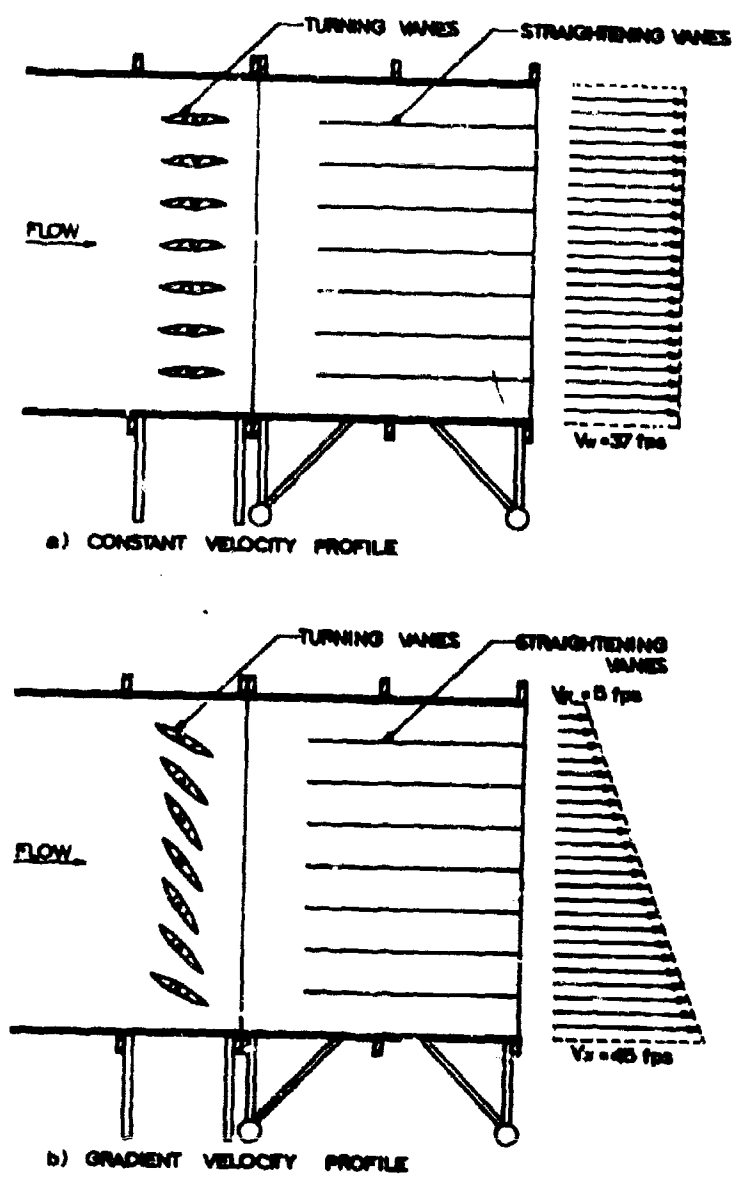


Fig 37. Method of Achieving Various Velocity Profiles in Cross Wind Tunnel

rate to be changed while the fan ran at a constant speed. For this purpose, servo controls were arranged for convenient velocity control.

D. Catapult

The available vertical space was insufficient to attain the desired terminal velocity conditions by free falling models. Therefore, a pneumatic catapult was arranged capable of accelerating 10 lbs to 100 ft/sec within a 2 ft stroke. A schematic diagram of this system is shown in Fig 38.

In operation, the parachute model is attached to the bottom of the catapult push rod, as shown in Fig 39. In this manner, the driving force is transmitted directly to the load, allowing the canopy to inflate as the system accelerates. Figure 39 shows the parachute ready for launching with 4 lines holding the canopy open for easy air inflation. This method proved to be very successful.

At launch, an electric device releases the pushrod-piston assembly which then moves under the force from compressed air stored in the reservoir above the piston. By varying the reservoir pressure, one can obtain the desired acceleration and the respective tunnel velocity conditions. After a stroke of approximately 2 ft, the piston impacts the polyurethane cushion which stops its movement and absorbs the kinetic energy. At this instant the parachute and load are released from the pushrod and enter subsequently the wind shear layer.

E. Experimental Procedure

The primary objective of the experiments was to obtain experimental data which could be compared with the theoretical predictions. For this purpose the parachute models were injected into the cross wind tunnel at speeds of 20, 30, and 40 ft/sec, which were also the equilibrium speeds of the system. These tests were all conducted in a constant wind layer of 37 ft/sec.

As in all experiments, a certain amount of error is introduced into each test. Hence, standard methods were followed to minimize experimental error such as averaging data and curve fitting. In view of this procedure, the results of Section III may be considered to be of acceptable accuracy.

The testing arrangement is schematically shown in Fig 40, while Fig 41 presents the entire arrangement.

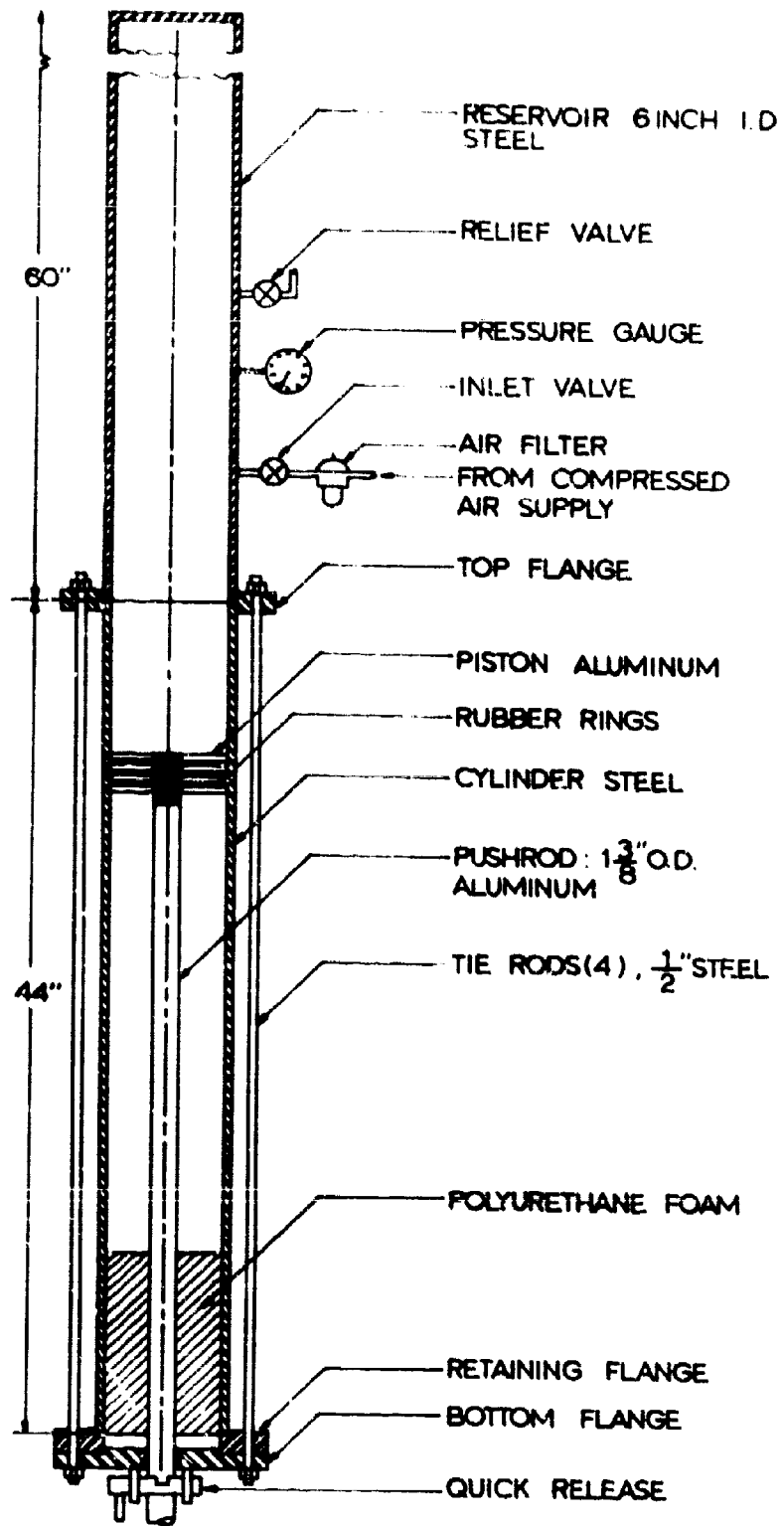


Fig 38. Pneumatic Catapult for Accelerating Parachutes to Terminal Velocity Conditions



Fig 39. Parachute Model in Launch Configuration

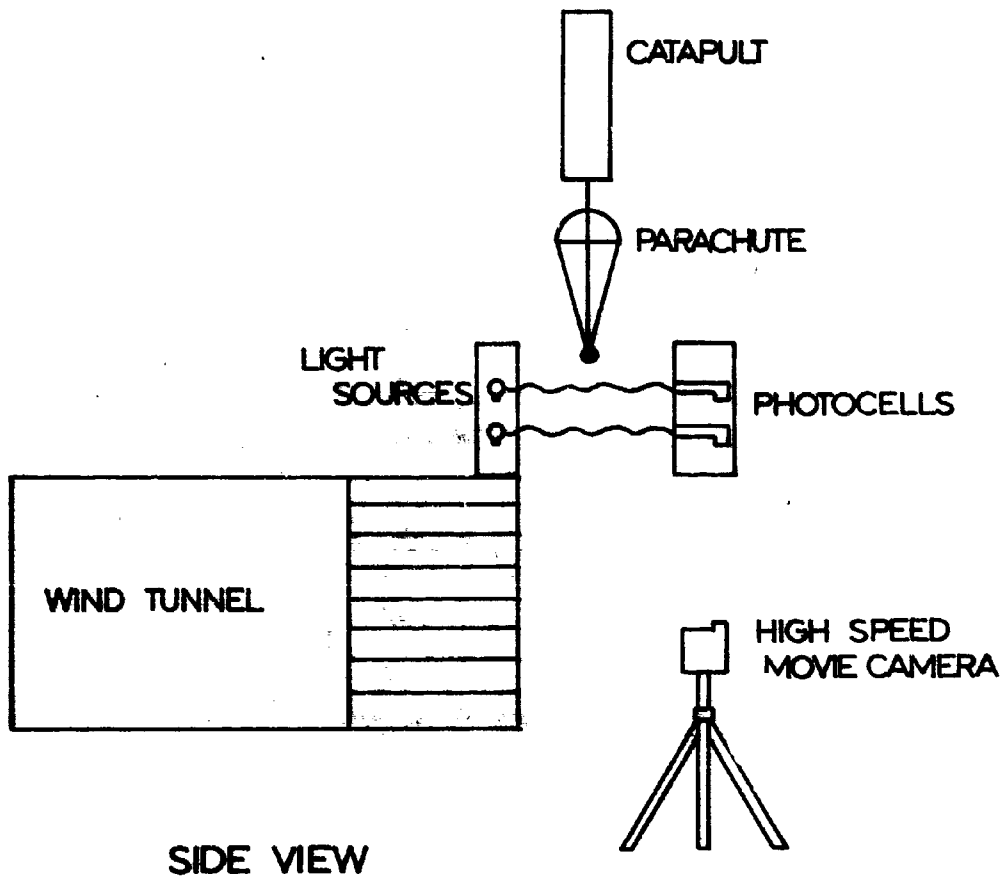
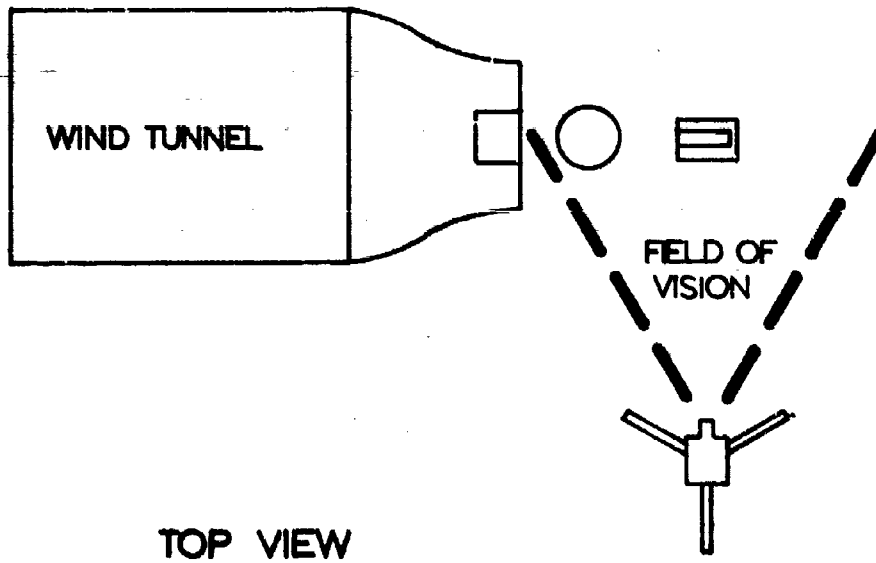


Fig 40. Experimental Set-Up for Determining Parachute Trajectories



Fig 41. Catapult Systems and Cross Wind Tunnel

The system is composed of the catapult, wind tunnel, high speed movie camera, photocells, and timing equipment. The timing equipment, shown in Fig 42, consisted of a light beam oscillograph, frequency generator, and an electronic counter. The purpose of this equipment was to determine the injection speed of the parachute as it passes the photocells.

Photographic coverage of the trajectory allowed one to determine instantaneous position, velocity and orientation of the parachute. A sequence typical of photographs, shown in Fig 43, indicates the rapid response of the parachute-load system to the cross wind. In general, the canopies collapsed slightly when entering the shear layer, but approach within a short time the angle of relative wind and assume a more regular form. Since the experimental wind shear layer was relatively thin, the parachutes did not fully return to a complete equilibrium, but the shown sequence pictures are characteristic for the parachute behavior in the initial phase of the trajectory.

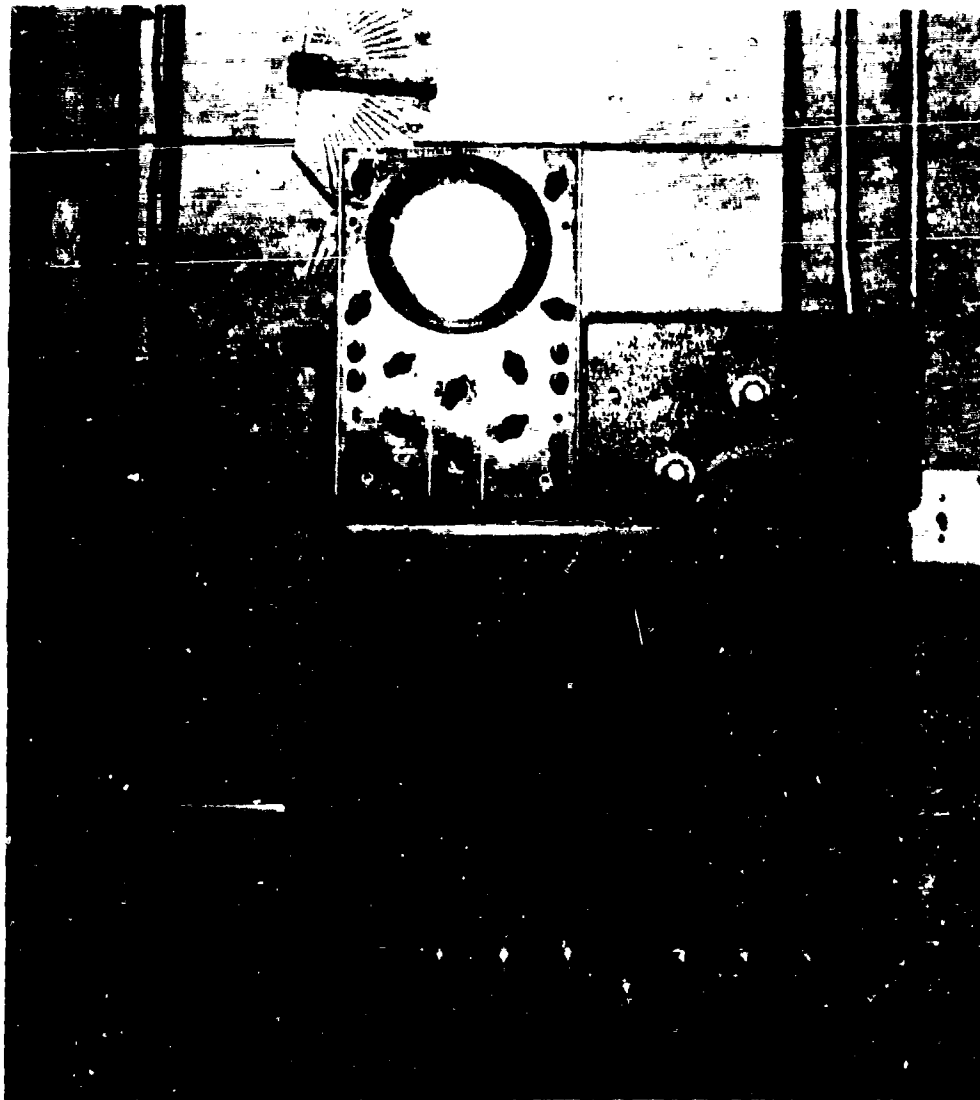


Fig 42. Timing Equipment for Determining Injection Velocities

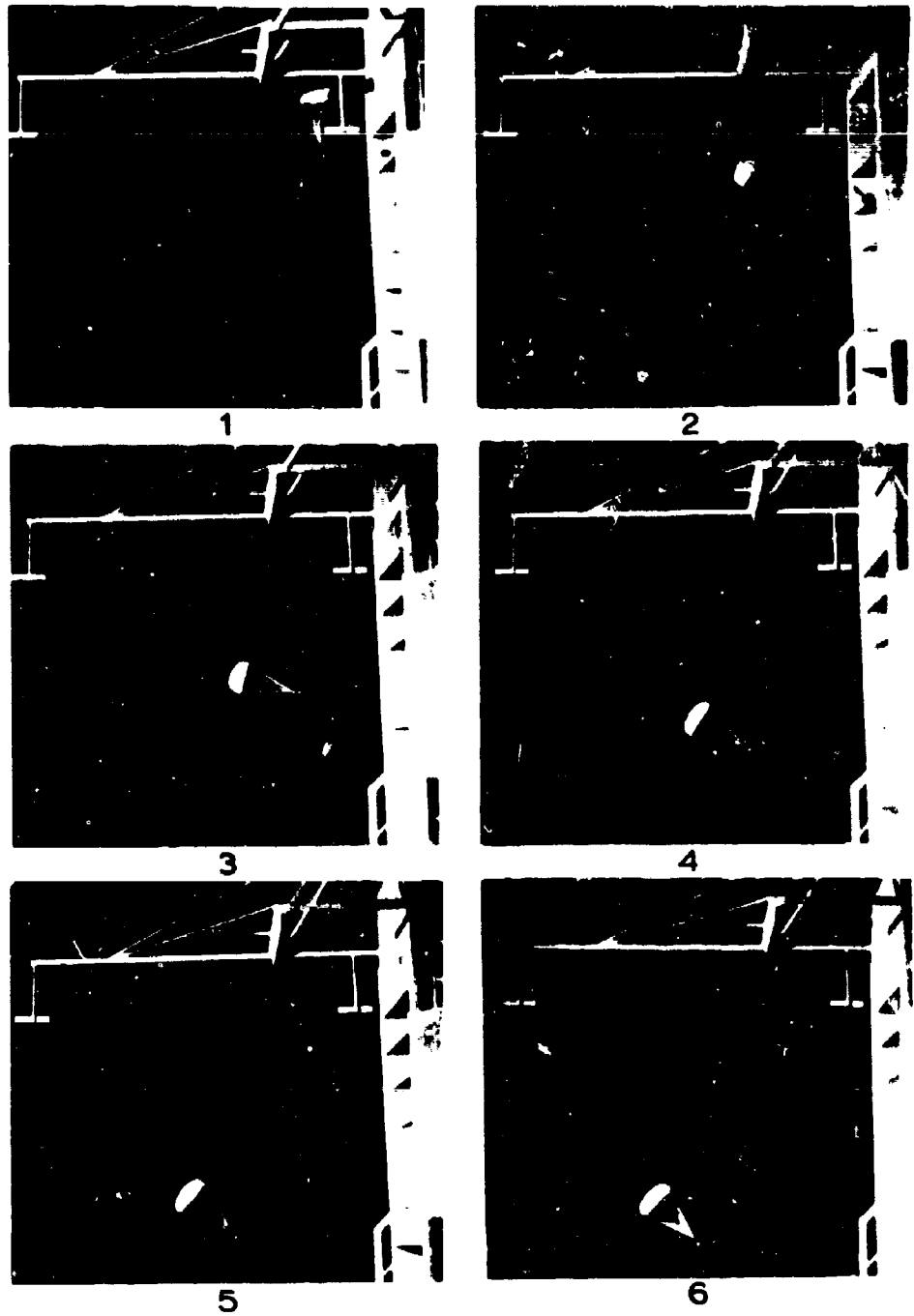


Fig 43. Photographic Sequence of Parachute Trajectory

V. REFERENCES

1. H. G. Heinrich and L. W. Rust. Dynamic Stability of a Parachute Point-Mass Load System, FDL-TDR-64-126, Flight Accessories Laboratory, Wright-Patterson Air Force Base, Ohio, February, 1964.
2. H. G. Heinrich and E. L. Haak. Stability and Drag of Parachutes with Varying Effective Porosity, ASD TDR 62-100, ASTIA AD 288572, Flight Accessories Laboratory, Wright-Patterson Air Force Base, Ohio, December, 1961.
3. H. G. Heinrich, L. W. Rust, E. L. Haak, and R. J. Niccum. Research and Development of Rigid, Rising Radar Reflective Balloons, Vol. I, "The Wind Response Error of an Ascending Balloon Under Consideration of Apparent Mass," sponsored by G. T. Schjeldahl Company, Northfield, Minnesota, July, 1963.
4. H. G. Heinrich. Chapter III - The Physical Process of Parachute Inflation, presented at the summer course on Aerodynamic Deceleration at the University of Minnesota, July, 1965.
5. Milne-Thomson. Theoretical Hydro-Dynamics, The MacMillan Company, New York, 1960.
6. H. G. Heinrich. Experimental Parameters in Parachute Opening Theory, presented at the 19th Symposium on Shock and Vibration, 1952.
7. Earl D. Rainville. Elementary Differential Equations, The MacMillan Company, New York, 1960.
8. Shukry K. Ibrahim. Experimental Determination of the Apparent Moment of Inertia of Parachutes, FDL-TDR-64-153, Flight Accessories Laboratory, Wright-Patterson Air Force Base, Ohio, December, 1964.
9. C. V. Eckstrom. Theoretical Study and Engineering Development of Jimsphere Wind Sensor, Monthly P. R. to NASA Marshall Space Flight Center, G. T. Schjeldahl, Northfield, Minnesota, December, 1964.

Unclassified
Security Classification

DOCUMENT CONTROL DATA - R&D		
<i>(Security classification of title, body of abstract and indexing annotation must be entered when the overall report is classified)</i>		
1. ORIGINATING ACTIVITY (Corporate author)	22. REPORT SECURITY CLASSIFICATION	
University of Minnesota Minneapolis, Minn. 55455	Unclassified	
	23. GROUP	n/a
3. REPORT TITLE		
Investigation of Cross Wind Effects on Stable Parachute-Point Mass Systems		
4. DESCRIPTIVE NOTES (Type of report and inclusion dates)		
Final Report April 65 - April 66		
5. AUTHOR(S) (Last name, first name, initial)		
McInrion, H. G. Nietz, T. C.		
6. REPORT DATE	79. TOTAL NO. OF PAGES	78. NO. OF REFS
November 1968	64	9
8a. CONTRACT OR GRANT NO.	8b. ORIGINATOR'S REPORT NUMBER(S)	
AF33(615)-2554	AFFDL-TR-66-105	
a. PROJECT NO.	8c. OTHER REPORT NO(S) (Any other numbers that may be assigned this report)	
6065		
c. Task No.		
606503		
16. AVAILABILITY/IDENTIFICATION NOTICES Qualified users may obtain copies of this report from the Defense Documentation Center. Release to CPSTI is not authorized. This document is subject to special export controls and each transmittal to foreign governments or foreign nationals may be made only with prior approval of the AF Flight		
17. SUPPLEMENTARY NOTES		18. SPONSORING MILITARY ACTIVITY
		AFFDL (FDFR) Wright-Patterson AFB, Ohio
19. ABSTRACT		
<p>The influence of horizontal wind shear layers upon descending, statically stable parachutes has been studied analytically and experimentally. The investigation is concerned with horizontal displacements, response velocity, response time, and angle of attack. For comparison, experiments were conducted with two circular flat ribbon, two ringslot, and one ribless guide surface parachute model. The results show that the analytical predictions are a satisfactory first approximation of the observed performance characteristics.</p>		

nn FORM 1473
JAN 64

Unclassified
Security Classification

14. KEY WORDS	LINK A		LINK B		LINK C	
	ROLE	WT	ROLE	WT	ROLE	WT
Parachutes Static stability Horizontal wind shear Displacement Steady descent Response velocity Response time						

INSTRUCTIONS

1. ORIGINATING ACTIVITY: Enter the name and address of the contractor, subcontractor, grantee, Department of Defense activity or other organization (corporate author) issuing the report.

2a. REPORT SECURITY CLASSIFICATION: Enter the overall security classification of the report. Indicate whether "Restricted Data" is included. Marking is to be in accordance with appropriate security regulations.

2b. GROUP: Automatic downgrading is specified in DoD Directive 5200.10 and Armed Forces Industrial Manual. Enter the group number. Also, when applicable, show that optional markings have been used for Group 3 and Group 4 as authorized.

3. REPORT TITLE: Enter the complete report title in all capital letters. Titles in all cases should be unclassified. If a meaningful title cannot be selected without classification, show title classification in all capitals in parenthesis immediately following the title.

4. DESCRIPTIVE NOTES: If appropriate, enter the type of report, e.g., interim, progress, summary, annual, or final. Give the inclusive dates when a specific reporting period is covered.

5. AUTHOR(S): Enter the name(s) of author(s) as shown on or in the report. Enter last name, first name, middle initial. If military, show rank and branch of service. The name of the principal author is an absolute minimum requirement.

6. REPORT DATE: Enter the date of the report as day, month, year; or month, year. If more than one date appears on the report, use date of publication.

7a. TOTAL NUMBER OF PAGES: The total page count should follow normal pagination procedures, i.e., enter the number of pages containing information.

7b. NUMBER OF REFERENCES: Enter the total number of references cited in the report.

8a. CONTRACT OR GRANT NUMBER: If appropriate, enter the applicable number of the contract or grant under which the report was written.

8b, 8c, & 8d. PROJECT NUMBER: Enter the appropriate military department identification, such as project number, subproject number, system numbers, task number, etc.

9a. ORIGINATOR'S REPORT NUMBER(S): Enter the official report number by which the document will be identified and controlled by the originating activity. This number must be unique to this report.

9b. OTHER REPORT NUMBER(S): If the report has been assigned any other report numbers (either by the originator or by the sponsor), also enter this number(s).

10. AVAILABILITY/LIMITATION NOTICES: Enter any limitations on further dissemination of the report, other than those

imposed by security classification, using standard statements such as:

- (1) "Qualified requesters may obtain copies of this report from DDC."
- (2) "Foreign announcement and dissemination of this report by DDC is not authorized."
- (3) "U. S. Government agencies may obtain copies of this report directly from DDC. Other qualified DDC users shall request through _____."
- (4) "U. S. military agencies may obtain copies of this report directly from DDC. Other qualified users shall request through _____."
- (5) "All dissemination of this report is controlled. Qualified DDC users shall request through _____."

If the report has been furnished to the Office of Technical Services, Department of Commerce, for sale to the public, indicate this fact and enter the price, if known.

11. SUPPLEMENTARY NOTES: Use for additional explanatory notes.

12. SPONSORING MILITARY ACTIVITY: Enter the name of the departmental project office or laboratory sponsoring (paying for) the research and development. Include address.

13. ABSTRACT: Enter an abstract giving a brief and factual summary of the document indicative of the report, even though it may also appear elsewhere in the body of the technical report. If additional space is required, a continuation sheet shall be attached.

It is highly desirable that the abstract of classified reports be unclassified. Each paragraph of the abstract shall end with an indication of the military security classification of the information in the paragraph, represented as (TS), (S), (C), or (U).

There is no limitation on the length of the abstract. However, the suggested length is from 150 to 225 words.

14. KEY WORDS: Key words are technically meaningful terms or short phrases that characterize a report and may be used as index entries for cataloging the report. Key words must be selected so that no security classification is required. Identifiers, such as equipment model designation, trade name, military project code name, geographic location, may be used as key words but will be followed by an indication of technical content. The assignment of links, rules, and weights is optional.